GOLD/ COPPER SULPHIDE AND GOLD NANOPARTICLES FOR APPLICATION IN CANCER THERAPY

by

SANTANA BALA LAKSHMANAN

Presented to the Faculty of the Graduate School of

The University of Texas at Arlington in Partial Fulfillment

of the Requirements

for the Degree of

MASTER OF SCIENCE IN MATERIALS SCIENCE & ENGINEERING

THE UNIVERSITY OF TEXAS AT ARLINGTON

December 2011

ACKNOWLEDGEMENTS

First and foremost, I would like to thank to my advisor Dr. Wei Chen for his guidance, support, patience, and encouragement all throughout my thesis work. I am extremely thankful to him for entrusting me with the responsibility of many exciting and challenging research projects to work on which helped me improve my research and analytical skills tremendously. Without his guidance and helpful suggestions, this work would not have been possible.

I would also like to thank Dr. Yaowu Hao and Dr. Fuqiang Liu for serving as committee members in reviewing my research work. My sincere thanks to all the professors in Materials Science and Engineering department for offering their knowledge and guidance. I would also like to appreciate the help from Ms. Jennifer Standlee and Ms. Libia Cuauhalti for helping me with all the department formalities and paper work. I am also thankful to Dr. Kwang Song for having collaborated with us on the Radiation project. I would like to extend my gratitude to Dr. Meng Tao and Dr. Kytai Truong Nguyen for permitting me to use some instruments in their lab.

I am extremely grateful to Dr. Marius Hossu and Dr. Xiaoju Zou for helping me with cell studies and laser treatment respectively and also for explaining and discussing the many issues that I came across during my research. I also want to thank postdoctoral scholars Dr. Lun Ma, Dr. Ke Jiang and visiting professor Dr. ZhongXin Liu for sharing their ideas in various perspectives. My heartfelt thanks to all the members in my group. I really enjoyed the time working with them.

Lastly but most importantly, I would like to offer my deepest thanks to my family and friends, for their unconditional love and support.

November 18, 2011

ABSTRACT

GOLD/ COPPER SULPHIDE AND GOLD NANOPARTICLES

FOR APPLICATION IN CANCER THERAPY

Santana Bala Lakshmanan, M.S.

The University of Texas at Arlington, 2011

Supervising Professor: Wei Chen

The main goal of this research is to use Gold/ Copper Sulphide (Au/ CuS) and Gold nanoparticles (AuNPs) for improving the therapeutic effects in the treatment of cancer. One of the biggest successes in photothermal therapy is the use of AuNPs which however has its own drawbacks i.e. it is expensive and that the NIR absorption of Au nanostructures is from surface plasmon resonance which is dependent on the dielectric constant of the surrounding matrix. Thus, the plasmon absorption maxima would shift for in-vivo observations compared to in-vitro. Alternatively, Copper Sulphide (CuS) nanoparticles, developed recently, have also been used for photothermal therapy. CuS nanoparticles are much cheaper than AuNPs, they have NIR absorptions around 900 nm which originates from the d–d transition of Cu^{2+} ions and hence it is not sensitive to size, shape or solvents, but their photothermal conversion efficiency is much lower than that of Au. Therefore, in this work, we combined the above two nanoparticle systems and developed a new type of agent – Au/ CuS core/shell nanoparticles that have better photothermal conversion efficiency and also overcome the limitations of the existing nanoparticle systems for photothermal therapy. TEM, EDS and UV-Vis-NIR results confirmed the CuS coating on AuNPs. From UV-Vis-NIR spectroscopy we obtained that these core/shell nanoparticles have their maximum absorbance at 981 nm in the NIR region thus making them

suitable for in vivo applications. Their absorption intensity was much higher than only Au and only CuS nanoparticles systems which in turn is responsible for their relatively high photothermal conversion efficiency. These core/ shell nanoparticles are also non-toxic and biocompatible and hence could be used for cell studies. Fluorescence properties of these Au/ CuS nanoparticles are an added advantage during photothermal treatment. They serve as fluorescent imaging agents for cancer cells and help in confirming the cellular uptake of nanoparticles. Photothermal studies proved the high photothermal conversion efficiency of Au/ CuS nanoparticles at laser powers much lower than the safety limit for human skin exposure.

Recently, AuNPs have also been studied as a radiation dose enhancement agent. Therefore, in our research we also investigated the AuNPs as a radiosensitizer in an orthotopic human prostate cancer rat model. As the first step towards this goal, preliminary studies were carried out at the in vitro level with AuNPs for radiation enhancement in three different cancer cell lines. AuNPs of an optimum size of 50 nm were synthesized and characterized. All the three cell lines showed different radiation enhancement effects upon irradiation with AuNPs and radiation enhancement was observed especially at lower doses.

TABLE OF CONTENTS

LIST OF ILLUSTRATIONS

Figure Page

CHAPTER 1

INTRODUCTION

1.1 Background on Cancer

Cancer is the third leading cause of death (after heart disease and stroke) in developed countries and the second leading cause of death (after heart disease) in the United States [1]. Because of the high death rate caused by cancer, plenty of research is going on in the field of Nanomedicine for Cancer diagnosis and therapy.

1.1.1 Tumor: Definition and Causes

Definition: "Tumor is an abnormal growth of body tissue. It can be cancerous (malignant) or non-cancerous (benign)" [2].

Causes: Generally tumors occur when there is a problem with the division of cells inside our body. Normally, the division of cells in the body is strictly controlled. If the balance of cell division and death is altered, a tumor may form.

Problems with the body's immune system can lead to tumors. Tobacco causes more deaths from cancer than any other environmental substance. Other causes include:

- Benzene and other chemicals and toxins
- Drinking excess alcohol
- Excessive sunlight exposure
- Genetic problems
- Inactivity (sedentary lifestyle)
- Obesity
- Radiation [2].

1.1.2 Growth of Tumors

A cancerous cell surrounded by healthy tissue will reproduce at a higher rate than the other cells, thereby affecting the nutrient supply and elimination of metabolic waste products. Once a small tumor mass is formed, the healthy tissue will not be able to compete with the cancer cells as there is no sufficient supply of nutrients from the blood stream. Tumor cells will displace healthy cells until the tumor reaches a diffusion-limited maximal size. This diffusion-limited maximal size of most tumors is around 2 mm^3 [3, 4, 5].

Generally tumor cells do not initiate apoptosis (a cell suicide mechanism) in a low nutrient environment as they do require oxygen, glucose and amino acids (building blocks of cell function). The healthy tissue which then becomes extinct did not demand high nutrients due to its slower growth rate. Thus the tumor cells will continue dividing because they do so without regard to nutrient supply but at the same time many tumor cells will also perish due to insufficient nutrients.

The tumor cells at the outer edge of a mass have the best access to nutrients while cells on the inside die creating a necrotic (death of cells) core within tumors that rely on diffusion to deliver nutrients and remove waste products.

In essence, a steady state tumor size forms, as the rate of proliferation is equal to the rate of cell death until a better link with the circulatory system is created. To grow beyond this size, the tumor must recruit the formation of blood vessels to provide the nutrients essential to fuel its continued expansion. Figure 1.1 shows the tumor development from a single cell to a diffusion-limited tumor.

There can be numerous tumors at this diffusion-limited maximal size throughout the body. Until the tumor can gain that admission to the circulation it will remain at this size and the process can take years. The exact molecular mechanisms that initiate angiogenesis (growth of new blood vessels from preexisting blood vessels) at a tumor site are not known and could be

unique to the site of origin but more information about what factors play a role in this process is being discovered [3].

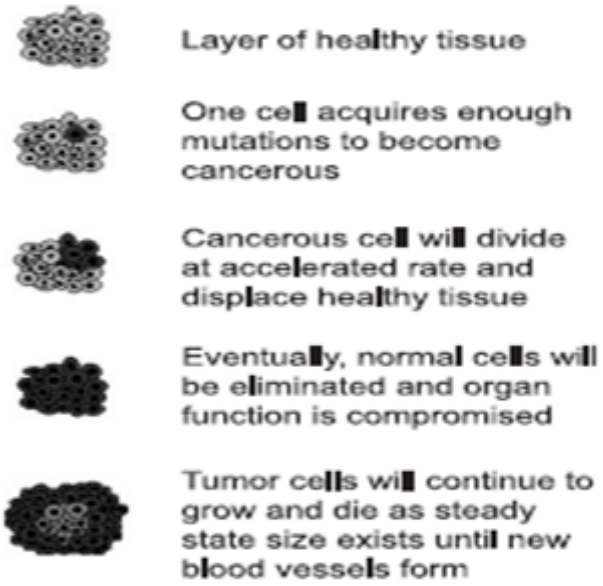

Figure 1.1 Tumor development from initial carcinogenesis to diffusion-limited maximal size [3]

1.1.3 Current Cancer Treatments

There are different types of treatment for patients with cancer. Some of the standard treatments used are discussed as follows [6-9]:

1.1.3.1 Surgery

Among all the treatments Surgery is the oldest form of cancer treatment. It as well plays an important role in diagnosing cancer and finding out how far it has spread (this process is called staging). For many types of cancer, surgery offers the greatest chance for cure. This works best, especially for cancers that have not spread to other parts of the body. Majority of the people with cancer will have some kind of surgery.

Preventive surgery: Preventive surgery is done to remove body tissue that is likely to become cancer, even though there are no signs of cancer at the time of the surgery. At times preventive surgery is used to remove an entire organ when a person has an inherited condition

that puts them at a much higher risk for having cancer some day. For example, some women with a strong family history of breast cancer have a higher risk of getting breast cancer. In such cases, these women may want to consider prophylactic mastectomy i.e. the breasts are removed before cancer is diagnosed.

1.1.3.2 Radiation Therapy

Radiation therapy is a cancer treatment that utilizes high-energy x-rays or other forms of radiation to kill cancer cells or keep them from growing. There are two types of radiation therapy 1) External radiation therapy and 2) Internal radiation therapy. In External radiation therapy a machine is used outside the body to send radiation toward the cancer. Internal radiation therapy uses a radioactive substance sealed in needles, seeds, wires, or catheters that are placed directly into or near the cancer. The way the radiation therapy is given depends on the type and stage of the cancer being treated.

1.1.3.3 Chemotherapy

Chemotherapy is a type of cancer treatment where drugs are used to stop the growth of cancer cells. These drugs either kill the cancer cells or prevent them from dividing. Chemotherapy is taken by mouth or by injecting it into the vein or muscle. These drugs go through the bloodstream and can reach cancer cells throughout the body. This is known as systemic chemotherapy. When chemotherapy is given directly into the spinal column, an organ, or a body cavity such as the abdomen, the drugs primarily affect cancer cells in those areas. This is known as regional chemotherapy.

1.1.3.4 Hormone therapy

Hormone therapy is a recently used treatment for cancer. In this type of treatment either the action of harmones are blocked or removed to stop the cancer cells from growing. Hormones are substances generated by glands in the body and circulated in the bloodstream.

1.1.3.5 Immunotherapy

Another recently used treatment for cancer is Immunotherapy. In this, patients are given medication to stimulate the body's immune system to fight cancerous cells.

1.1.4 Limitations on Current Cancer Treatments

All cancer treatments come with benefits, risks, and side effects. The types and intensity of side effects differ from person to person and with the type and location of the cancer, and the person's health. Downside of the current cancer treatment methods are discussed below [17-21]:

1.1.4.1 Radiation therapy Limitations

As radiation is a local treatment, side effects depend on the area of the body being treated. Some of the most common side effects are minor burns, skin changes, fatigue, loss of appetite, nausea, vomiting, weakness, and lowered resistance to infections.

1.1.4.2 Cancer Surgery Limitations

Common side effects of cancer surgery are: pain, swelling around the site of surgery, bleeding, bruising around the site of surgery, infection, fatigue, loss of appetite, etc.

1.1.4.3 Chemotherapy Limitations

Following are the common chemotherapy side effects that are common to several classes of chemo agents: nausea and vomiting, hair loss, fatigue, reduced blood levels of red blood cells, white blood cells or platelets, reduced or absent menstruation (periods) in women, changes in thinking and memory, sore and inflamed throat and mouth, brittle or discolored nails, diarrhoea or constipation, etc. Some long term side effects could be permanent organ damage to heart, lung, liver, kidneys, or reproductive system. In some people cognitive functions (such as thinking, concentrating, and memory) remain a challenge even after months or years after treatment. In addition, nervous system changes can develop months or years after the treatment.

1.1.4.4 Hormone Therapy Limitations

In Hormone therapy certain drugs have a high risk of developing a blood clot. Hormone therapy for prostate cancer can cause impotence. Hormone treatment for breast cancer can cause hot flushes and abnormalities in menstruation.

1.1.4.5 Immunotherapy Limitations

Some of the common immunotherapy side effects include itches and irritation around the injection area. Some other less common immunotherapy side effects are major swelling, bruising, cold, asthma or hay fever symptoms in a few hours after the injection and increased tiredness in the proceeding days after having the injection.

1.2 Gold Nanoparticles for Cancer Treatment

In the recent years, Gold nanoparticles (AuNPs or GNPs) have been brought to the front position of cancer research because of their simplistic synthesis procedures, rich surface chemistry, strongly enhanced and tunable optical properties and exceptional biocompatibility. High quality, yield and size controllable AuNPs can be prepared from simple citrate reduction method. We can also make different shapes of AuNPs like gold nanorods, gold nanoshells, hollow gold nanoparticles etc. These different shaped AuNPs show large red shift properties, thereby making them favorable candidates for Cancer Therapy [10].

1.2.1 Importance of AuNPs

There are quite a lot of reasons for the use of AuNPs in cancer nanotechnology which are listed as follows:

- Gold compounds have been used for medicinal purposes for over a long period of time in the history (In the past, over 5000 years ago, Egyptians consumed gold for mind, body and spiritual purification).
- There are several ways to synthesize AuNPs which are simple, cheap, safe and reliable.

- Different size AuNPs ranging from 2nm - 500nm can be synthesized by simply modifying the reaction parameters.
- Different shapes of AuNPs like spheres, rods, tubes, wires, ribbons, plate, cubic, hexagonal, triangular can also be synthesized by using templates and changing the reaction conditions.
- Surface modification of AuNPs using several biomolecules is easily possible due to the presence of a negative charge, which are highly reactive, on its surface. Another reason why AuNPs can be easily modified is that there is strong interaction between the gold surface and thiol/amine containing molecules like organic molecules, DNA, protein, enzyme, etc.
- AuNPs have a unique optical as well as electronic behavior due to the presence of surface plasmon resonance (SPR) bands. This explains why they are used in diagnosis and cancer therapeutics.
- It is well established that AuNPs are biocompatible and non-toxic.

In recent times, several literatures and groups have proved the efficiency of AuNPs to improve cancer treatment [11].

1.2.2 Bioconjugate Chemistry of AuNPs

Bulk gold is inert, but AuNPs show high chemical reactivity. The reason why AuNPs are frequently mentioned in nanomedicinal research is because of its rich surface chemistry. The rich surface chemistry of AuNPs permits surface modification reactions with large varieties of chemical and biochemical vectors to adapt to the needs of biomedical applications including imaging and therapy of cancer. AuNP-conjugates are made by the interaction of AuNPs with chemical functionalities present on simple chemical molecules or specific molecules of biological interest like biomolecules including peptides and proteins [12]. These AuNPs-conjugates labeled with tumor seeking ligands provide efficient site specific delivery of nanoparticles carrying imaging and therapeutic probes to target cancer cells.

There are lots of ways to synthesize AuNPs, mostly starting from commercial $HAu^{III}Cl_4$. Citrate reduction of Au^{III} to Au^0 in water is a method that is still used. According to our biological interest the citrate ligand of the AuNPs can be replaced by appropriate ligands. Some reasons for conjugating AuNPs with appropriate ligands are for targeting the drug or therapeutics to a specific site, to improve the stability of the AuNPs and to prevent their aggregation, to provide remedy to AuNPs that are capped with ligands that are cytotoxic, etc. [13, 14].

AuNPs can be stabilized using a variety of stabilizers like ligands, surfactants, polymers, dendrimers, biomolecules, etc. But the simplest way to stabilize AuNPs is by using thiolates where a strong Au–S bond between the soft acid Au and the soft thiolate base is farmed [13, 15].

AuNP solutions are bright red/purple colored owing to plasmon absorption. There is a shift in the plasmon absorption for any surface modification of AuNPs. Thus, this change in optical property can be used to confirm surface modifications of AuNPs [12].

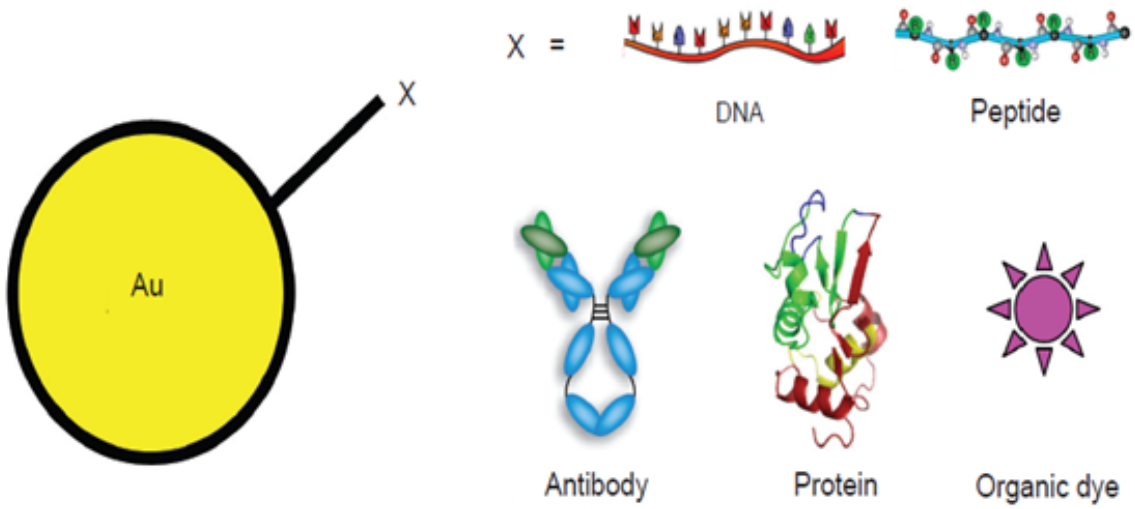

Figure 1.2 AuNPs bioconjugation with various molecules [1]

1.2.3 Surface Plasmon Resonance of AuNPs

The excitation of surface plasmons by light is denoted as a surface plasmon resonance (SPR) for planar surfaces or localized surface plasmon resonance (LSPR) for nanometer-sized metallic structures. Surface plasmons (SPs), are coherent electron oscillations that exist at the interface between any two materials where the real part of the dielectric function changes sign across the interface (e.g. a metal-dielectric interface, such as a metal sheet in air). The origin of this phenomenon was explained by Mie in 1908 by solving Maxwell's electromagnetic equation for the interaction of Light with Spherical particles.

According to his theory, for spherical nanoparticles that are much smaller than the wavelength of light (diameter d << λ), an electromagnetic field at a certain frequency (υ) induces a resonant, coherent oscillation of the metal free electrons across the nanoparticles. This oscillation is known as surface plasmon resonance which lies at the visible frequencies for Gold, Silver and Copper [16].

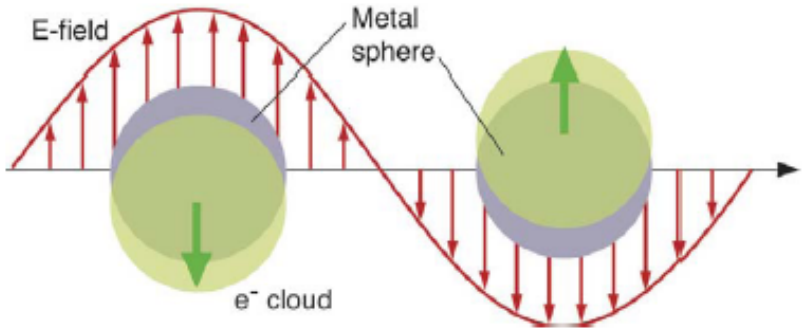

Figure 1.3 Schematic of the interaction of a metal nanosphere with light [16]
(The electromagnetic field of the light induces a coherent dipolar oscillation of the metal conduction electrons across the nanoparticles)

In metal nanoparticles, the localized surface Plasmon resonance consequences in an enhanced electromagnetic field at the metal nanoparticle surface. This in turn allows strong enhanced absorption and scattering of electromagnetic radiation in resonance with the SPR frequency of the noble metal nanoparticles, giving them intense colors and optical properties. AuNPs give rise to both absorption and scattering whose proportions depend upon the size of

AuNPs. When the size of the AuNP is 20nm absorption is seen, whereas when the size is 40 nm scattering starts to show up. The surface Plasmon resonance band of Au NPs is dependent on the size, composition, shape, inter-particle distance and environment (dielectric properties) of the AuNPs. It is the high sensitivity to these factors that makes AuNPs basis for their use in biological labeling, detection, diagnostic and sensing [10, 13, 16].

1.2.4 Application of AuNPs in Cancer Nanotechnology

AuNPs are used in cancer nanotechnology for Cancer Imaging, Photothermal therapy, Radiation therapy and Targeted delivery of therapeutics.

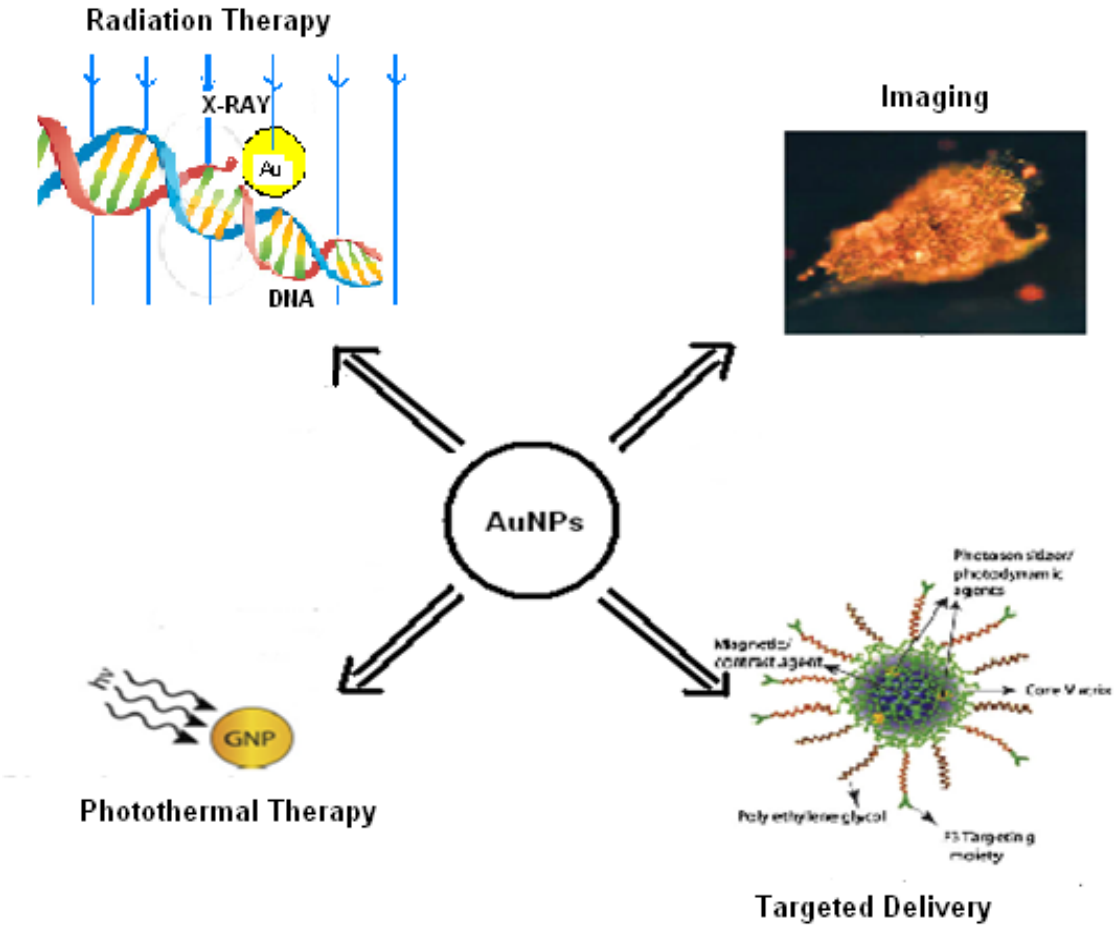

Figure 1.4 Applications of AuNPs in Cancer Nanotechnology [12, 22, 23, 24]

Of all the many application of AuNPs in cancer treatment, Photothermal therapy and Radiation therapy will be discussed as they are the main focus of my research.

1.2.4.1 AuNPs for Photothermal Therapy (PTT)

The mainstream treatments used for treating cancer are chemotherapy, surgical removal and radiotherapy. Nevertheless, all these treatments have their own drawbacks like chemotherapy has numerous side effects, surgery is limited to huge, accessible tumors and radiotherapy is highly invasive to healthy tissues alongside the radiation path. To overcome these issues laser hyperthermia i.e Photothermal therapy was used as a mild alternative for cancer treatment. Photothermal therapy is the use of optical heating for ablation of tumors [13, 16]. Upon heating between 40 and 45℃ cancer cells are damaged while preventing the surrounding cells from being affected [30].

Using Organic photoabsorbers (dyes) such as indocyanine green and inorganic ones such as iron oxide for PTT required high radiation energy because of their small absorption cross sections (Absorption cross section is a measure for the probability of an absorption process). In the case of Iron Oxide, high quantities of iron oxide was needed which by itself is more or less toxic. To overcome these shortcomings AuNPs were used for PTT. AuNPs are non-toxic with high absorption cross sections requiring minimal irradiation energy. Their high absorption cross section is due to their optical properties resulting from surface plasmon absorption. The absorption cross-section of Au nanoparticles (C_{abs} ~ 2.9 x 10^{-15} m^2 per mole for 40 nm spheres with an absorption band around 530 nm) is five orders of magnitude larger than that of indocyanine green (C_{abs} ~ 1.7 x 10^{-20} m^2 per mole with an absorption band around 800 nm) [13, 16, 22, 26].

Upon irradiating Surface Plasmon Resonance of AuNPs, fast conversion of light into heat takes place in about 1ps [28, 29]. Small AuNPs of size 10-30nm are delivered more easily to cancer cells through different methods like conjugation with antibodies, physiological transportation, etc. Once they are delivered these AuNPs form self assembled large clusters

directly inside cells. This results in laser-induced bubble formation that is more effective for killing cells. Moreover, SPR shift from visible region to near infra red region is seen [13, 16].

El-Sayed et al proved that immunotargeted Au Nanospheres are efficient photothermal agents for *in vitro* living cells. Carcinoma cell lines, HOC and HSC, overexpress EGFR protein which is labeled successfully by means of 40 nm AuNPs conjugated to anti-EGFR antibodies. Dark-field microscopy images of the cancer cells are taken to confirm the labeling of cancer cells. On the other hand, healthy HaCaT cells show relatively nonspecific nanoparticle labeling. A 514 nm excitation from continuous-wave (CW) argonion laser was used for PTT to excite the SPR band of the nanoparticles centered at 530 nm. To see what happens to the cells upon photothermal irradiation, the cells were stained with trypan blue dye. The dye accumulated carefully only in dead cells staining them blue, while live cells were clear under the microscope. Within 4 mins the HOC and HSC cancer cell lines experienced photothermal damage at laser energy thresholds 19 W/cm^2 and 25 W/cm^2 respectively. This is infact less than half of that of healthy HaCaT cells (57 W/cm2). There was no photothermal damage of any other cell lines without Au nanoparticles-conjugate up to laser energies of 76 W/cm^2 [25, 27].

“Thus effective targeting of Au nanoparticle bioconjugates specifically to cancer cells, combined with the high absorption cross section of the nanoparticles in the laser excitation region, facilitates selective photothermal cancer therapy at a low enough laser energy that the benign cells remain undamaged ” [25].

1.2.4.2 AuNPs for Radiation Therapy

Radiotherapy remains a main modality of cancer therapy. Delivering a curative dose of radiation to tumor tissues while sparing normal tissues is still a great challenge in radiation therapy. Radiation is used in radiotherapy since radiation (X-rays, γ-rays and fast-moving charged particles such as ions, electrons and protons) interacts with DNA inside living cells causing enough damage and that could lead to cell death. As radiation travel through matter they produce ions, radicals and free electrons. These electrons in turn produce large number of

second generation of radicals, ions and free electrons. According to most of the studies DNA is damaged indirectly by hydroxyl radicals [39]. Nevertheless, the electrons can also cause damage to DNA. Low-energy electrons emitted from metal films also caused DNA strand breaks directly [40].

The theory of using high atomic number (Z) materials to enhance the dose given to a tumor during radiation therapy was introduced over 20 years ago. Earlier attempts were made using iodine. However, the use of gold as a radiosensitizer shows potential than the former attempts using iodine. This is because gold has an atomic number higher than iodine and has greater biocompatibility [24]. Some of the potential advantages of AuNPs over iodine are listed as follows:

- At 20 and 100 keV gold absorbs approximately 3 times more than iodine.
- Gold is relatively inert and biocompatible.
- For gold, the range of the enhancing effect can be more than several cells, say 100 *m*m, Therefore it is not necessary that gold is delivered to all tumor cells.
- Depending on the energy of beam and amount of gold delivered the dose enhancement factor for gold can be 1.2 to >5.
- Small molecules (such as iodine) clear the blood quite quickly than nanoparticles. Nanoparticles can stay in the blood for hours if designed to do so, thus enhancing the chances of reaching the tumor site through enhanced permeation and retention.
- AuNPs can be synthesized over a wide range of sizes (1–1000 nm) and designed for best tumor penetration and delivery.
- AuNPs have a rich surface chemistry, permitting flexible design and multifunctionality by integrating varied ligands for most advantageous properties.
- Before a therapeutic dose is delivered imaging the biodistribution of gold is possible. This in turn is useful for planning the treatment and quantifying the prediction of dose enhancement.

- Effectual tumor targeting with antibodies, peptides or drugs may be achievable with nanoparticles. Target sites on tumor cells are limited and one or a few iodine atoms per antibody do not deliver enough high-Z material. On the contrary, one antibody attached to a 15-nm AuNP would deliver 70 000 gold atoms [45].

Carter et al. performed Monte Carlo calculation to understand the mechanism behind enhanced sensitization properties of AuNPs. They pointed out that to cause this phenomenon the following effects can be combined: (1) enhanced localized absorption of X-rays by nanostructures; (2) effective release of low-energy electrons from AuNPs; and (3) efficient deposition of energy in water in the form of radicals and electrons. When AuNPs are present, the electrons released from these nanoparticles could create more radicals [24].

A study in 2000 by Herold et al showed a dose enhancement effect for cells suspended in gold microspheres solution and also for tumors injected with gold microspheres. Since the gold particles were in micro size they could not penetrate into the cells. Hence, in order to overcome this issue AuNPs of size between 1-100nm were used. The factors that affect radiation enhancement are size of the NPs, concentration of NPs, and cell type. Recent studies show that there is an enhancement in radiosensitization when GNPs are internalized in cancer cells. Even 24 hrs after irradiation of cells with internalized NPs an enhancement in DNA double strand breaks (DSBs) was seen. Thus, it is accepted as true that the size of the NPs plays a big role in cellular uptake leading to different sensitization properties [41, 42].

Hainfeld *et al.* conducted experiments *in vivo* to explore the enhancement effect of AuNPs and the data showed the potential utility of AuNPs for cancer X-ray therapy. They demonstrated that tumor bearing mice injected with AuNPs could be completely eradicated off tumor in 30 days after irradiation with 250 kVp X rays. It is believed that a larger portion of the energy of the primary ionizing photons is transferred to the tumor due to the increased absorption of X rays by GNPs. The detailed mechanism behind this is still unknown.

Nevertheless, this work by Hainfeld et. al remains a milestone in the field of radiation therapy [24].

Recently, Chang et al. combined clinical electron beams with a lower concentration of AuNPs in tumor bearing mice to demonstrate the possibility of obtaining dose enhancement effects. 1 g/kg concentration of AuNPs was injected intravenously into the mice instead of 2.7 g/kg (as per Hainfeld et al.) but still higher accumulation was reported within the tumor compared to tumor periphery when the irradiation was done 24 hrs post-AuNP injection. The reason for this was owing to enhanced permeability and retention effect, which takes benefit of the poorly formed tumor vasculature [43]. The AuNPs could also be surface modified for preferential targeting of cancer cells [44].

1.3 CuS nanoparticles for Photothermal therapy

Besides AuNPs and carbon nanotubes, semiconductor copper sulphide (CuS) is a latest developing and promising photothermal agent for cancer therapy due to its low cost, low cytotoxicity and intrinsic NIR region absorption. Semiconductor CuS nanostructures display interesting electrical, optical and catalytic properties. They offer several advantages over AuNPs. They are much less expensive than gold. They also have a NIR absorption which originates from the *d–d* transition of Cu^{2+} ions unlike surface plasmon resonance in gold nanostructures [31]. CuS nanoparticles can be used for *in vivo* applications *due to the d–d* transition peaks at 900 nm, which is in the NIR range [30].

Chen et al. developed CuS nanoparticles as a new agent for photothermal ablation of cancer cells in in vitro under an irradiation of 808 nm laser with a power of 16 and 24 W/cm^2. This suggests that CuS nanomaterials have a great potential to revolutionize photothermal agents. However, one of the serious limitations of CuS nanoparticles as photothermal agents is their low photothermal conversion efficiency. In addition, the 808 nm laser power intensity (16 and 24 W/cm^2) required to cause sufficient cell death in the *in vitro* monolayer setting is approximately 48 and 72 times higher than the safety limit (~ 0.33 W/cm2) of 808 nm laser

intensity setting for human skin exposure. This fact makes a great barrier for *in vivo* application of the CuS nanoparticles and 808 nm lasers. To address this issue, recently Qiwei Tian et al. reported CuS superstructures for photothermal therapy where they had used 980nm laser for the treatment. They claimed that even at a very low laser power of 0.51 W/cm^2 the cancer cells can be killed in the presence of these CuS superstructures. But they had no quantitative data showing the percentage cell viability after photothermal treatment to prove the efficiency of their CuS superstructures [30, 37].

1.4 Overview of Research project

My research is mainly focused on the application of Au/ CuS and AuNPs in the treatment of cancer. Towards the achievement of this goal, two projects were carried out. They are:

1. Au/ CuS core/shell nanoparticles for Photothermal therapy and Imaging. This work has been discussed in chapter 2.
2. Preliminary studies for the investigation of AuNPs as a radiosensitizer in an orthotopic human prostate cancer rat model. This work has been discussed in chapter 3.

CHAPTER 2

GOLD/COPPER SULPHIDE CORE/SHELL NANOPARTICLES FOR PHOTOTHERMAL THERAPY AND IMAGING

2.1 Introduction

One of the biggest recent successes in photothermal therapy is the use of AuNPs because of its rich surface chemistry, surface plasmon absorption properties and easy synthesis techniques. Different shapes of AuNPs such as gold nanorods, gold nanoshells and hollow gold nanoparticles can also be easily synthesized as they are favorable candidates for in vivo NIR (near infrared) photothermal therapy [10]. But it does have some disadvantages like the NIR absorption in gold nanostructures is from the surface plasmon resonance. This surface plasmon absorption peak of gold nanostructures is dependent upon the dielectric constant of the surrounding matrix. Thus, when they are delivered to the cancer cells, the plasmon absorption maximum will shift compared with in vitro observations. This might complex the treatment conditions [30].

On the other hand, CuS nanoparticles, developed recently, have also been used for photothermal ablation of tumor cells. The advantage of this over gold nanostructures is that they are much less expensive than gold. They also have a NIR absorption which originates from the *d–d* transition of Cu^{2+} ions unlike surface plasmon resonance in gold nanostructures [31]. CuS nanoparticles can be used for *in vivo* applications *due to the d–d* transition peaks at 900 nm, which is in the NIR range. Though it offers many advantages over gold nanostructures it does have a severe limitation. These CuS nanoparticles have relatively low photothermal conversion efficiency. Thus, the concentration of CuS nanoparticles and the laser energy required to cause sufficient cell death in the *in vitro* monolayer setting are prohibitively high for *in vivo* applications [30].

Thus, the goal of my research was to design a core/shell nanostructure that would overcome the limitations of the existing nanoparticle systems for photothermal therapy. In my design, AuNP (core) is coated with CuS (shell) to form the core/shell nanostructure. The idea behind designing a core/shell structure is to combine the effects of many materials into one ultimate material which unites the properties needed for the various applications. Due to the *d–d* transition peaks at 900 nm for CuS (shell) the Au/CuS core/shell structure can be used for in vivo application without having to worry about the plasmon absorption shift of AuNPs in *in vitro* and *in vivo* conditions. These Au/ CuS core/shell nanoparticles have absorption intensity much higher than only Au or only CuS nanoparticles systems because of which they have better photothermal conversion efficiency. Furthermore, these nanoparticles should also act as fluorescent imaging agents for cancer cells due to the formation of metal – ascorbic acid complexes in the solution. Thus, in this chapter we will discuss the synthesis, characterization and application of Au/ CuS core/shell nanoparticles in imaging and photothermal cancer therapy.

2.2 Materials and Methods

2.2.1 Materials

Sodium Borohydride ($NaBH_4$, Acros), Chloroauric acid ($HAuCl_4$, Aldrich Chemical company), Cetyltrimethylammonium Bromide (CTAB, Sigma Chemical Company), Ascorbic acid (Sigma Chemical company), Nickel Nitrate ($Ni(NO_3)_2.6H_2O$, Alfa Aesar), Thiobenzoic acid (Sigma Aldrich), Silver Nitrate ($AgNO_3$, Sigma Chemical Company) , Copper Nitrate ($Cu(NO3)_2$, Aldrich Chemical company), Copper Chloride ($CuCl_2 \cdot 2H_2O$, Sigma Aldrich), Thioglycolic Acid (TGA, Sigma Aldrich), Sodium hydroxide (NaOH, Sigma Aldrich), Thioacetamide (Aldrich Chemical Company).

2.2.2 Synthesis of nanoparticles

2.2.2.1 Synthesis of AuNPs

Au nanopolyhedra were grown using the seeded growth method. Specifically, the seeds were made by the addition of a freshly prepared, ice-cold 0.01 M NaBH4 solution (0.6 mL, 0.006 mmol) into a mixture solution composed of 0.01 M HAuCl4 (0.25 mL, 0.0025 mmol) and 0.1 M CTAB (7.5 mL, 0.75 mmol). The resultant solution was mixed by rapid inversion for 2 min and was then kept at room temperature for 1 h before use. The growth solution was prepared by the sequential addition of 0.1 M CTAB (6.4 mL, 0.64 mmol), 0.01 M HAuCl4 (0.8 mL, 0.008 mmol), and 0.1 M ascorbic acid (3.8 mL, 0.38 mmol) into water (32 mL). The CTAB-stabilized seed solution was diluted 10 times with water. The diluted seed solution (0.02 and 0.06 mL) was then added into the growth solution for the growth of Au nanocubes and nanopolyhedra, respectively. The resultant solution was mixed by gentle inversion for 10 s and then left undisturbed overnight [32, 33].

2.2.2.2 Coating AuNPs with CuS

0.002 g (0.0060 mmol) of nickel thiobenzoate i.e $(PhCOS)_2Ni$ (prepared using $Ni(NO_3)_2{\cdot}6H2O$, thiobenzoic acid and $AgNO_3$ [32]) was dissolved in 10mL of washed Au nanopolyhedra dispersion prepared previously. This was followed by the addition of 0.01 M $Cu(NO3)_2$ solution. The concentration of Cu^{2+} in the solution was controlled to be 300μM. The resultant mixture solution was transferred into an autoclave and heated at 140 ℃ for 3 h [32]. Similarly, two more samples were prepared with 100μM and 200μM concentration of Cu2+ in the solution for comparison purposes. After removing the container from autoclave it was left overnight at room temperature to cool down, after which the nanoparticle solution was dialyzed to remove all the unreacted chemicals.

2.2.2.3 Synthesis of Thioglycolic acid (TGA) stabilized CuS nanoparticles

A total of 0.017048 g of $CuCl2{\cdot}2H2O$ (0.1 mmol) was dissolved in 100 ml of distilled water, 0.2 mmol of TGA (~14.2 μl) was added into the solution under constant stirring and the

pH was adjusted to 9.0 by drop-wise addition of a 1 M solution of NaOH. The solution was placed into a three necked flask fitted with a septum and valves, and was degassed by argon bubbling for 20 min. A solution of thioacetamide (8.0 mg, 0.1 mmol) in distilled water (20 ml) was added, and the whole solution was heated at 50°C for 2 h to promote nanoparticle growth [30].

2.2.3 Characterization of nanoparticles

2.2.3.1 TEM and EDS

10 µl of the Au/ CuS nanoparticle solution was placed onto the copper grid for HRTEM observations. The nanoparticles were allowed to settle down and dried on the grid before analyzing the sample on TEM instrument. Energy dispersive X-ray spectroscopy (EDS) was used to carry out the elemental analysis. The HRTEM images and EDS spectrum of the particles were obtained with a Hitachi 9500 electron microscope with accelerating voltage of 300 kV.

2.2.3.2 UV-Vis-NIR Spectroscopy

The absorption measurements were made using JASCO V-570 UV-Vis- NIR Spectrophotometer. The absorption spectra were compared between Au, CuS and Au/ CuS core/shell nanoparticles. The TGA stabilized CuS nanoparticles were diluted to 100µM, 200µM, and 300µM concentration for comparison with similar concentrations of Cu^{2+} in Au/ CuS nanoparticle solution. Based on the wavelength at which the peaks were obtained the Au/ CuS nanoparticle formation can be confirmed. The absorption intensities were also compared between samples.

2.2.3.3 Fluorescence studies

Pictures of Au and Au/ CuS core/shell nanoparticles were taken under normal light and UV light (360nm) using a Canon EOS REBEL T2i camera.

Different samples of ascorbic acid were prepared for fluorescence studies. The first sample of Ascorbic acid solution was prepared in deionized (DI) water and aged for 5 months.

The second sample of ascorbic acid was prepared in tap water and left at room temperature for 5 days. Finally, the third sample of ascorbic acid was prepared in tap water and kept at 65℃ for 1 day. Pictures of these three samples were taken under normal light and UV light (360nm) using a Canon EOS REBEL T2i camera.

To measure the fluorescence emission spectra, ascorbic acid samples were prepared in DI and tap water with a concentration similar to the concentration used during the synthesis of Au and Au/ CuS nanoparticles. The fluorescence emission spectra were measured for these samples that were – freshly prepared, stored at 4℃ for 1 day, stored at room temperature for 1 day and stored at 65℃ for 1 day. Along with these Au and Au/CuS nanoparticles solutions were also measured using a Shimadzu RF-5301PC fluorescence spectrophotometer.

2.2.4 Cell Culture and Cell viability Assay

In this study, breast cancer - MCF-7 cells (Michigan Cancer Foundation – 7) were used to evaluate the photothermal ablation and fluorescence imaging ability of Au/ CuS core/ shell nanoparticles. Before conducting photothermal ablation and imaging studies, MTT assay was done to study the toxicity of the nanoparticles.

Cell culture: The cells were washed 3 times with PBS (37ºC) followed by replacement with medium. MCF-7 cells were seeded onto a 96-well plate with a density of 2000 cells per well (with 90 µL medium) and incubated for 48 hours at 37℃ and 5% CO_2. After incubation, it was observed under a microscope (ZEISS IM-35) to see if the cell were attached before treatment with nanoparticles.

Nanoparticle treatment: The cultured cells were incubated with control (PBS - Phosphate-buffered saline) and 25% of the concentration of Au/ CuS nanoparticle solution (this is the highest concentration of the nanoparticle solution used in photothermal therapy and imaging) for 24 hours at 37℃ and 5% CO_2.

Cell viability assay: MTT assay was used to determine the cell viability. 10µl of 5mg/ml MTT solution was added to each well and Incubated for 4 hours at 37℃ and 5% CO_2. The

supernatant was then removed and cells are lysed with 100 µl DMSO. Using a microplate reader absorbance was recorded at 570nm to determine cell survival.

2.2.5 In vitro fluorescence imaging

MCF-7 cells were cultured as described in section 2.2.4 and incubated with 10% concentration of the original nanoparticle solution of Au and 10% concentration of the original nanoparticle solution of Au/ CuS at 37℃ and 5% CO_2 for 24 hours. Fluorescence imaging was done on the following day using an Olympus DP72 fluorescence microscope.

2.2.6 In vitro photothermal ablation of cancer cells with Au/ CuS core/ shell nanoparticles

The cells were cultured as described in section 2.2.4 and incubated with 25%, 10% and 2.5% concentration of the original Au/ CuS nanoparticle solution at 37℃ and 5% CO_2 for 24 hours. After incubation was completed, the culture media with nanoparticles were removed and resupplied with fresh media. The cells were then irradiated with a 980nm NIR laser (Opto Engine LLC) at an output power of 0, 0.125 or 0.2 W/cm^2 for 5mins. After irradiation, the culture media was removed and resupplied with fresh media and MTT assay was carried out to know the cell viability after irradiation.

Imaging was also done to see the number of living and dead cells after photothermal treatment. In this case the cultured cells were incubated with 25%, 10% and 2.5% concentration of the original Au/ CuS nanoparticle solution at 37℃ and 5% CO_2 for 24 hours. After incubation, the culture media with nanoparticles were removed and resupplied with fresh media. The cells were then irradiated with a 980nm NIR laser at an output power of 0, 5, 10 or 20 W/cm^2 for 5mins. In this, a higher output power is required for the complete burning of cells. The cells were then washed with PBS and stained with calcein AM for visualization of live cells and with Ethidium Homodimer-1 (EthD-1) for visualization of dead cells, according to the manufacturer's suggested protocol (Invitrogen). The cells were imaged under an Olympus DP72 fluorescence microscope.

2.3 Results and Discussion

2.3.1 CuS coating of AuNPs

CuS coating on AuNPs was confirmed from HRTEM images shown in figure 2.1. Crystal lattice fringes from (102) and (103) lattice planes could be observed. The lattice spacing of the (103) plane measured from figure 2.1.a is approximately 0.282 nm and that of the (102) plane measured from figure 2.1.b was approximately 0.30 nm. These results are very close to the lattice spacing of the (103) plane (0.282 nm) and of the (102) plane (0.305 nm) of previously reported hexagonal CuS nanostructures [30, 34, 35]. Thus this proves that the shell was composed of small protruding flakes of hexagonal crystalline CuS.

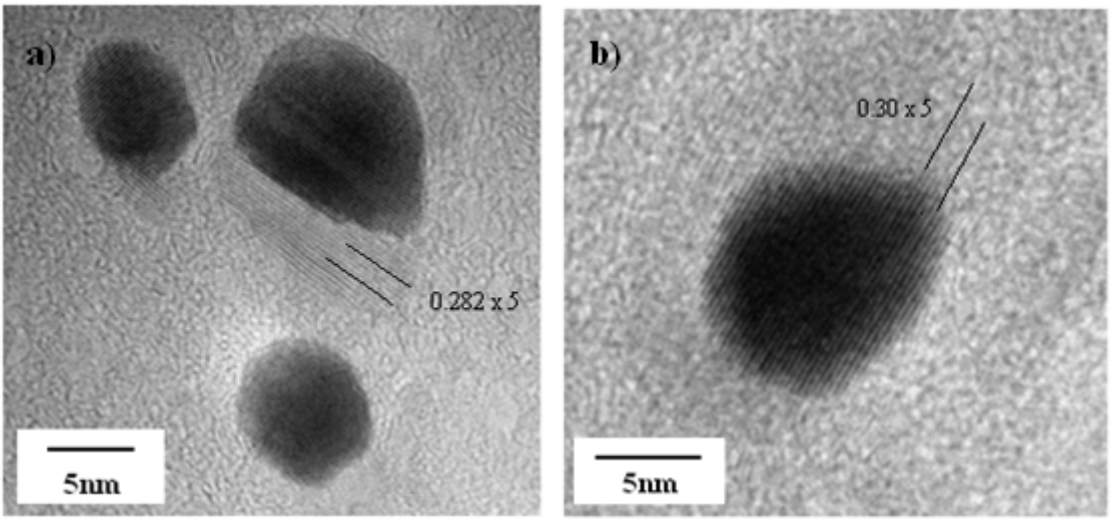

Figure 2.1 HRTEM images of Au/ CuS nanoparticles

The EDS spectrum (Figure 2.2) measured at the shell shows peaks confirming the presence of Cu and S. We suppose that the peaks from Al and Fe were introduced by the impurities from copper grid, TEM system or the preparation procedure. This result thus demonstrates the CuS coating of AuNPs.

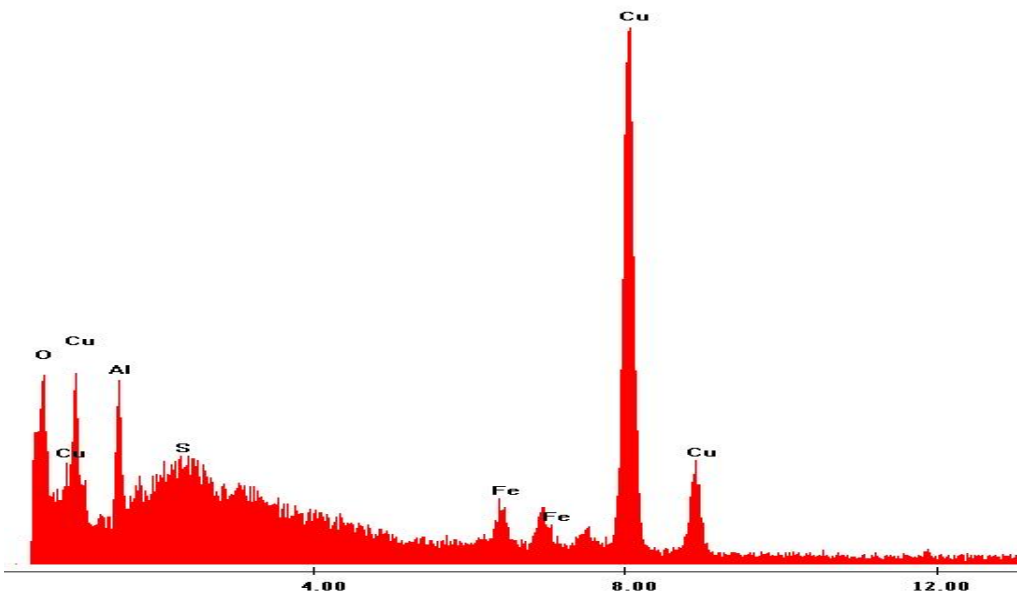

Figure 2.2 EDS spectrum measured at the shell of Au/ CuS nanoparticles

Results obtained from UV-Vis-NIR spectroscopy are shown in figures 2.3, 2.4 and 2.5. In these measurements, AuNPs (which were used as precursors for the synthesis of Au/ CuS nanoparticles) and TGA stabilized CuS nanoparticles were used as references for comparison with Au/ CuS nanoparticles.

The AuNPs had a peak at 524nm and TGA stabilized CuS nanoparticles had a peak at 990nm. From literatures it was found that Au nanospheres display a single absorption peak in the visible range between 510 nm and 550 nm [1]. The literatures also have it that the CuS nanoparticles have their absorption peak in the NIR region around 930nm [38]. The results obtained match with the data already available in literatures and hence these nanoparticles could be used as references for Au/ CuS nanoparticles.

The absorption spectrum of Au/ (CuS - 100μM) nanoparticles seemed to follow a pattern similar to CuS nanoparticles in the NIR region and AuNPs in the visible region. Their absorption peaks at 531nm and 981nm matched with the peaks of AuNPs (524nm) and CuS

(990nm) nanoparticles respectively. The slight change in their peak absorption wavelengths could be attributed to the formation of the core/ shell structure. These results once again confirmed the formation of Au/ CuS core/shell nanoparticles.

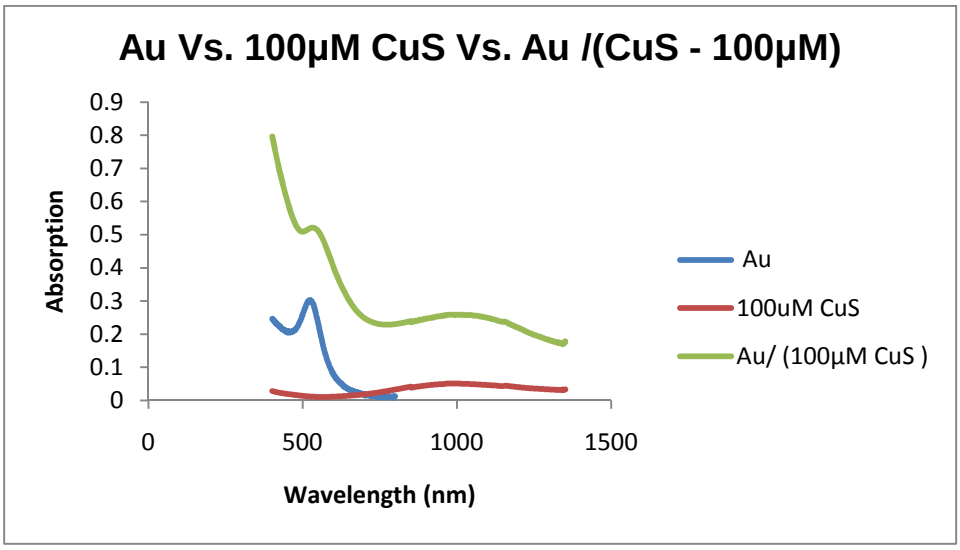

Figure 2.3 UV-Vis-NIR Absorption Spectrum: Au vs. 100µM CuS vs. Au / (CuS - 100µM)

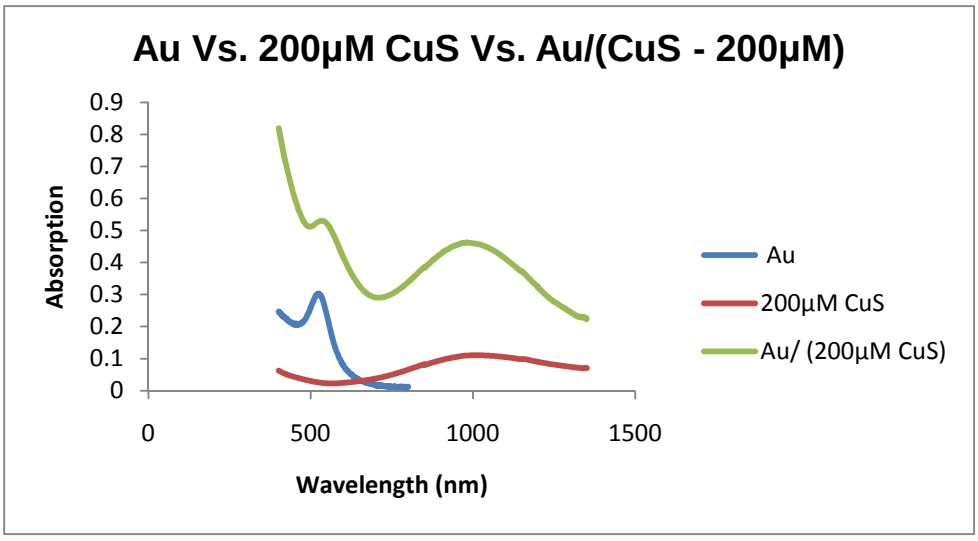

Figure 2.4 UV-Vis-NIR Absorption Spectrum: Au vs. 200µM CuS vs. Au / (CuS - 200µ)

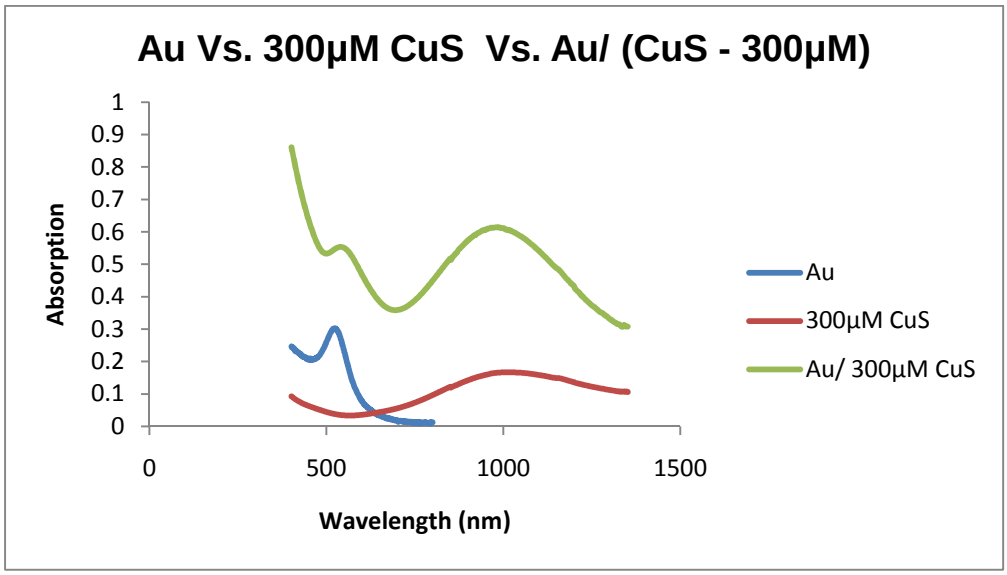

Figure 2.5 UV-Vis-NIR Absorption Spectrum: Au vs. 300µM CuS vs. Au / (CuS - 300µM)

The absorption intensities of Au/ CuS nanoparticles are much higher than only Au or only CuS nanoparticles at similar concentrations (calculated based on precursors). It also shows that as the concentration of Cu^{2+} in the Au/ CuS nanoparticle solution increases the absorption intensity also increases strongly. Au/ (CuS - 300µM) nanoparticle solution was the one with highest absorption intensity of all the nanoparticle solutions and hence chosen for rest of the studies. Despite of having NIR absorption the issue with TGA stabilized CuS nanoparticles is their poor absorbance. Due to poor absorbance of CuS nanoparticles their photothermal conversion efficiency was low. This issue was overcome by Au/ (CuS - 300µM) nanoparticles which had a high absorption intensity and hence chosen for photothermal studies.

2.3.2 Fluorescence Studies

Here we found an interesting phenomenon. The Au and Au/ CuS solutions were found to be fluorescent as shown in figure 2.6.

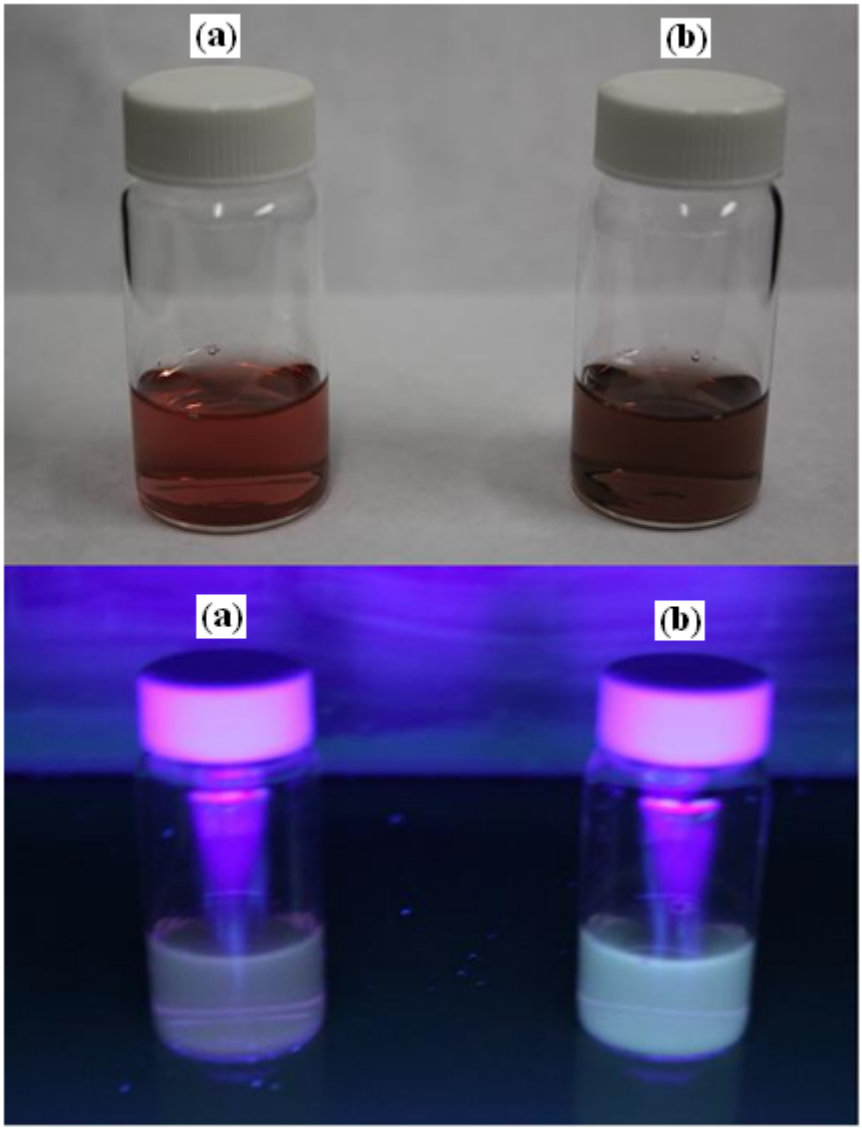

Figure 2.6 Fluorescence of Au and Au/ CuS nanoparticle solutions
Top: Normal Light; Bottom: UV Light (360nm)
(a) AuNP solution, (b) Au/ CuS nanoparticle solution

Our hypothesis is that, the fluorescence form Au/ CuS nanoparticle solution was due to the presence of Ascorbic acid. It has been previously reported that fluorescent metal nanoclusters can be formed when small molecules like L-ascorbic acid are used as reducing agents and stabilizing ligands. The ascorbic acid stabilizes the metal to form metal – ascorbic acid complexes which are fluorescent [36]. This is similar to our case, where we had used L-

ascorbic acid as a mild reducing agent during the synthesis of Au and Au/ CuS nanoparticles. In order to further understand the fluorescence from metal – ascorbic acid complexes a simple experiment was carried out with three different samples of ascorbic acid as described in 2.2.3.3

Pictures were taken for the different samples of ascorbic acid under normal and UV light as shown in Figure 2.7. The reason why samples were prepared in DI and tap water is that they have traces of metals present in them. Tap water has more traces of metals compared to DI water. In this study, we wanted to see if ascorbic acid formed complexes with metal traces present in DI and tap water to give fluorescence. We also wanted to study if temperature would affect the process of metal – ascorbic acid complex formation.

Figure 2.7 shows the fluorescence from the three different ascorbic acid samples. The fluorescence from these samples suggested the formation of metal – ascorbic acid complexes. The ascorbic acid sample (a) in DI water stored for 5 months at room temperature is yellowish - orange in color and the sample (b) in tap water stored @ 65℃ for 1 day is greenish – yellow in color under UV light. The sample (c), ascorbic acid in tap water kept at room temperature for 5 days, did not show much luminescence but had a slight greenish- yellow color under UV light. On comparing samples (b) and (c) which were prepared in tap water, sample (b) shows much better luminescence intensity than sample (c). This is because sample (b) was stored at a higher temperature (65℃ for 1 day) when compared to sample (c) which was stored at room temperature. This shows the effect of temperature in the formation of metal- ascorbic acid complexes. It also agreed with a previously reported work which stated that the yield of metal-ascorbic acid complexes is strongly affected by the reaction conditions such as temperature and concentration [36]. The sample (a) prepared in DI water and left at room temperature took a long time to form the metal – ascorbic acid complexes to give fluorescence. This is due to the fact that it was stored at room temperature and DI water has less trace of metals compared to tap water to form complexes.

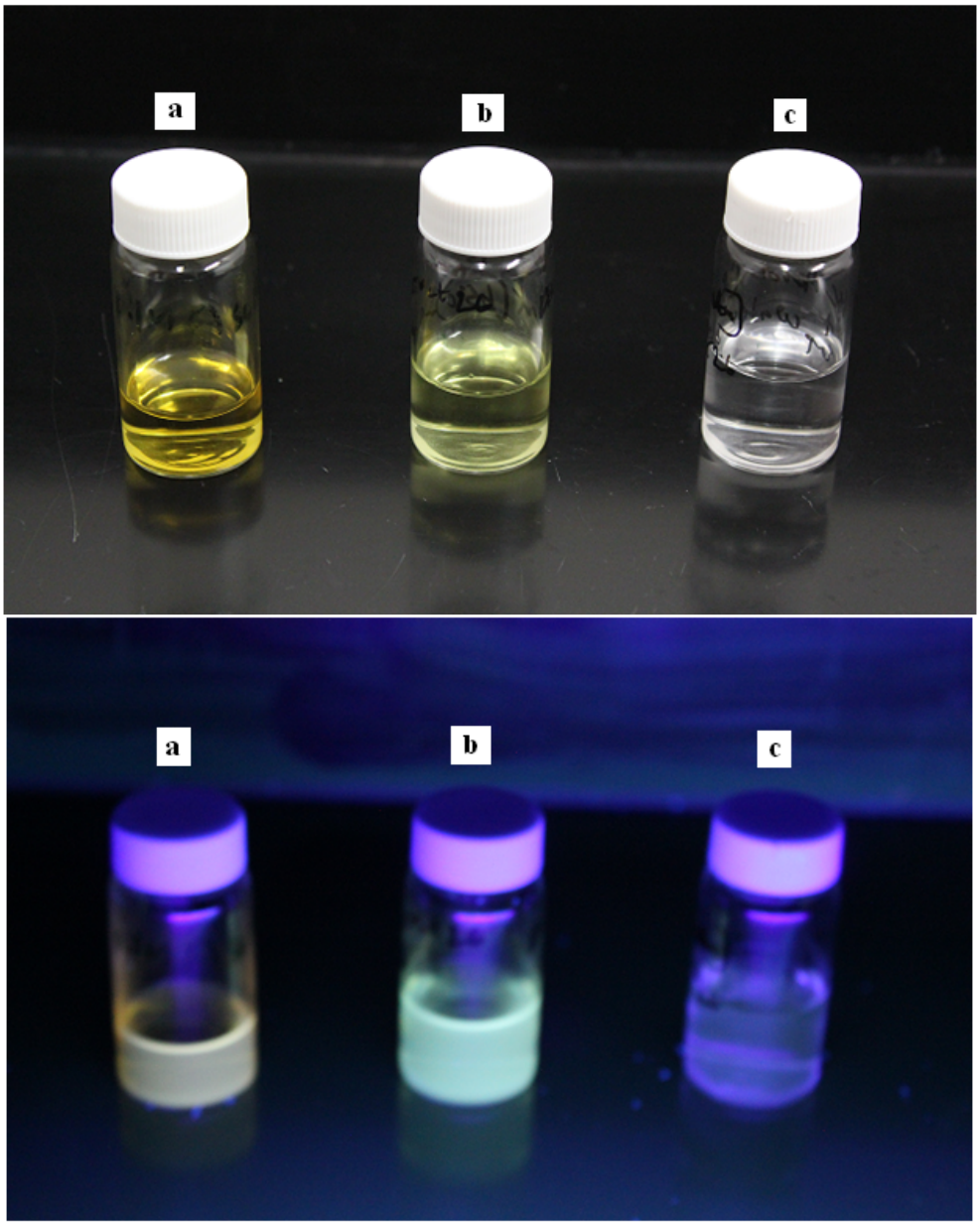

Figure 2.7 Fluorescence of Ascorbic Acid samples
Top: Normal Light; Bottom: UV Light (360nm)
(a) 5 months old Ascorbic Acid solution in DI water, (b) Ascorbic Acid solution in tap water @ 65℃ for 1 day. (c) Ascorbic Acid solution in tap w ater kept at room temperature for 5 days

Fluorescence emission spectra (for an excitation wavelength of 426nm) of Au, Au/ CuS nanoparticle solutions and different ascorbic acid samples are shown in Figure 2.8. The peak fluorescence intensity of these samples (at 500 nm) is shown in Figure 2.9. Ascorbic acid

samples in DI water did not have much fluorescence intensity except for the slight increase in the one stored at 65℃ for 1 day. The fluorescence intensity of ascorbic acid samples in tap water were slightly better than the respective ones in DI water except for the one stored at 65℃ for 1 day were the intensity was much higher. The reason for this could be due to the fact that tap water has more traces of metals than DI water to form complexes with ascorbic acid and give the fluorescence. Higher temperatures seemed to accelerate the formation of metal-ascorbic nanoclusters thereby showing an increase in fluorescence intensity. Thus, as reported in a previous work we have also observed fluorescence from metal - ascorbic acid nanoclusters.

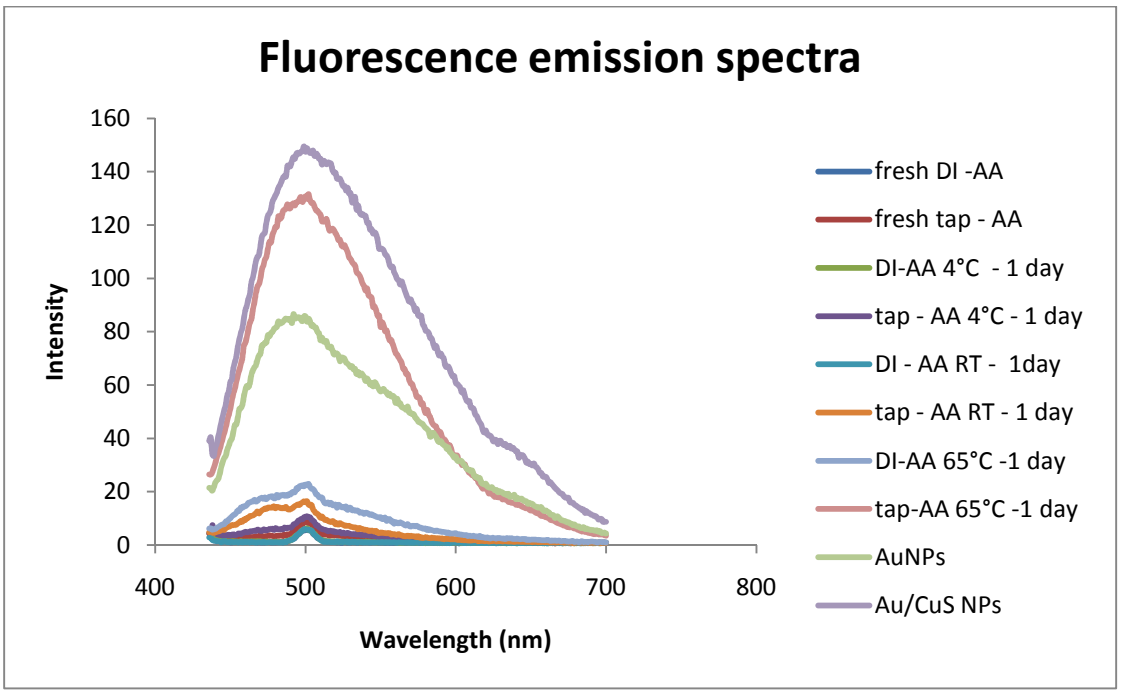

Figure 2.8 Fluorescence emission spectra of Au, Au/ CuS and different ascorbic acid samples (AA – Ascorbic acid, RT – room temperature, DI – DI water, tap – tap water)

The fluorescence emission spectra (Figure 2.8) seemed to be very broad especially for Au, Au/CuS and ascorbic acid sample in tap water kept at 65℃ for 1 day. As suggested before this could be due to the presence of multiple emisive species [36]. When different size nanoclusters are formed (say Au – ascorbic acid complexes were formed with either 2

molecules or 6 molecules of ascorbic acid attached to the nanoclusters) the fluorescence emission spectra tends to broaden.

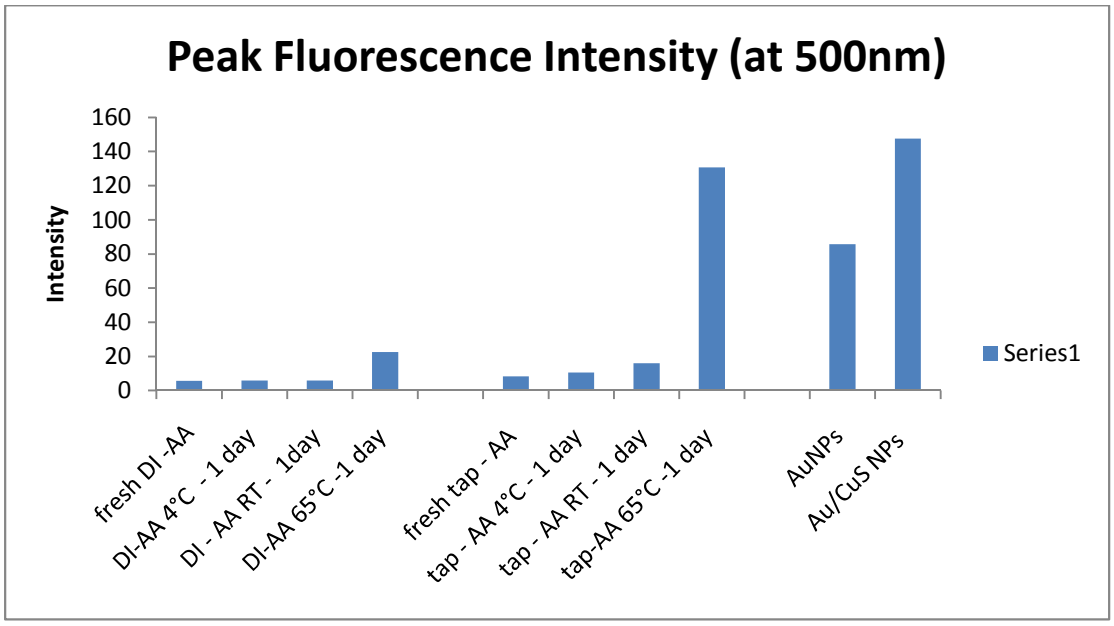

Figure 2.9 Intensity of fluorescence at the peak (500nm) for Au, Au/ CuS and different ascorbic acid samples (AA – Ascorbic acid, RT – room temperature, DI – DI water, tap – tap water)

2.3.3 Cytotoxicity of Au/ CuS nanoparticles

Cytotoxicity study was carried out for the highest concentration of Au/ CuS nanoparticle solution used during photothermal therapy and imaging. 25% concentration of the original Au/ CuS nanoparticle solution was the highest concentration used for our studies. Figure 2.10 shows cell viability for control (PBS) and 25% Au/ CuS nanoparticle solution. Results are presented as mean ± standard error. Similar cell viability was observed for control and Au/ CuS nanoparticles. Thus, from this result we can conclude that Au/ CuS nanoparticles are non – toxic and biocompatible.

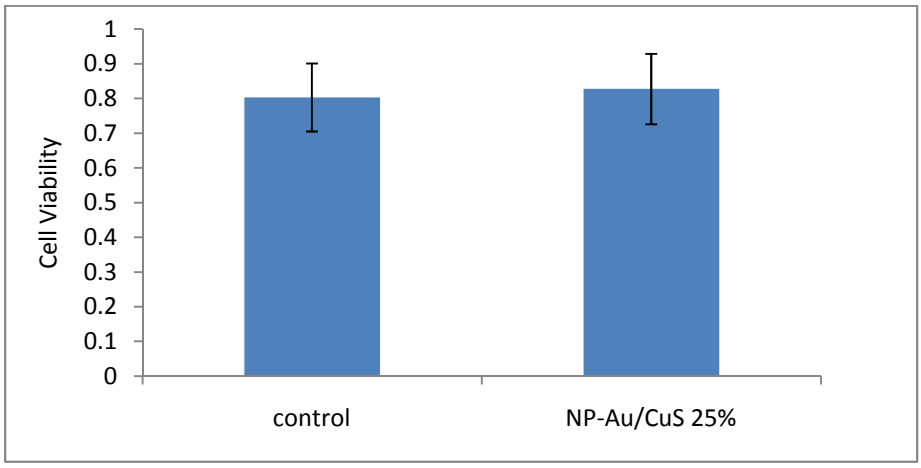

Figure 2.10 Cytotoxicity Study of Au/ CuS nanoparticles

2.3.4 In vitro Fluorescence imaging

Owing to the fluorescence properties of Au and Au/ CuS nanoparticles, they were used for in vitro fluorescence imaging (Figures 2.11 and 2.12).

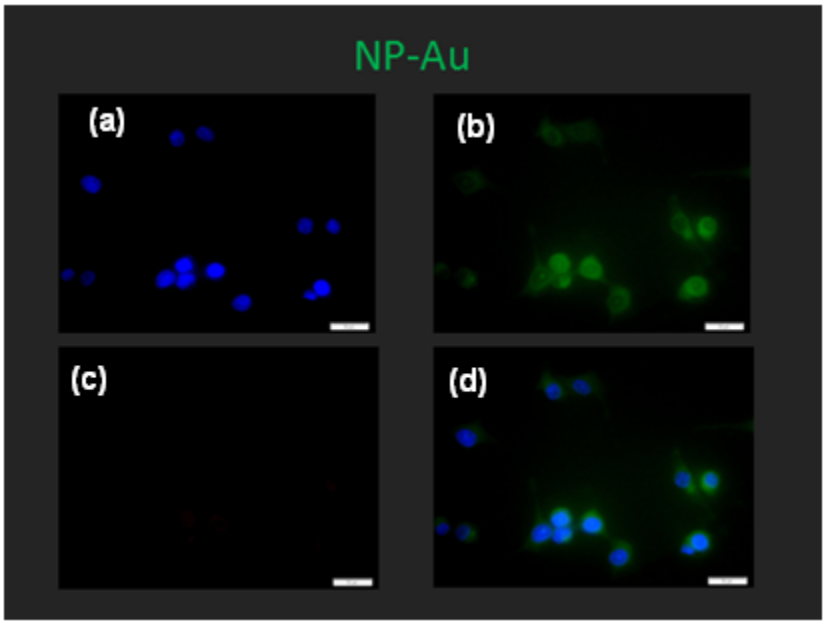

Figure 2.11 In vitro fluorescence imaging with AuNPs

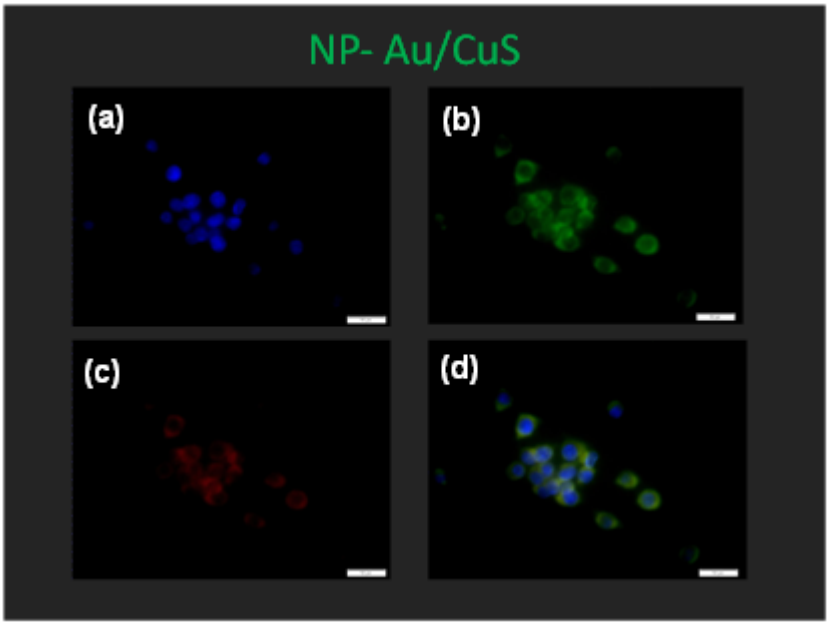

Figure 2.12 In vitro fluorescence imaging with Au/ CuS nanoparticles

These studies were carried out with MCF-7 breast cancer cells. DAPI or 4',6-diamidino-2-phenylindole is a fluorescent stain that was used to stain the nucleus (Blue color). DAPI can pass through an intact cell membrane therefore it can be used to stain both live and fixed cells. In figures 2.11 and 2.12, (a) shows the nucleus of the cell stained with DAPI, (b) shows the image when excited at a wavelength of 510nm, (c) shows the image when excited at a wavelength of 595nm and (d) shows the merged image of (a), (b) and (c). Due to the fluorescence emission peak at 500nm for both Au and Au/ CuS nanoparticles, strong green emission was observed (when excited at 510nm) during in vitro fluorescence studies of both these nanoparticles. Due to the presence of red shift (because of the presence of multiple emissive species) in the emission spectra of these nanoparticles a less intense red emission was also observed in the the case of Au/ CuS nanoparticles (when excited at 595nm).

This fluorescence from nanoparticles, in the cytoplasm of cells, proved the fact that they have been uptaken by the cells. In using nanoparticles for cancer therapy, it is quite important to know that the cellular uptake of nanoparticles before we do any kind of treatment. Hence these

Au and Au/ CuS nanoparticles proved to be useful for fluorescence imaging and verifying the cellular uptake of nanoparticles. Upon targeting these nanoparticles they could also be used as fluorescent labels to the cancer cells in vivo.

2.3.5 Photothermal therapy with Au/ CuS nanoparticles

Photothermal therapy with Au/ CuS nanoparticles was carried out with three different laser output powers (5W/cm^2, 10W/cm^2 and 15W/cm^2) and three different concentrations (2.5%, 10% and 25% of the original concentration of Au/CuS). A 980nm NIR laser was used in this study as Au/ CuS nanoparticles had an absorption maximum at 981nm (in the NIR region). Their advantage over 808nm lasers is that they can penetrate deeper into biological tissues. Additionally, the safety limit of 980 nm laser intensity set for human skin exposure is ~ 0.726 W/cm2, which is twice more than that of 808 nm lasers (~ 0.33 W/cm2) [37]. In this study, imaging was done to see if the cells were living or dead cells after photothermal treatment. Calcein and EthD-1 stains were used for staining the living and dead cells respectively.

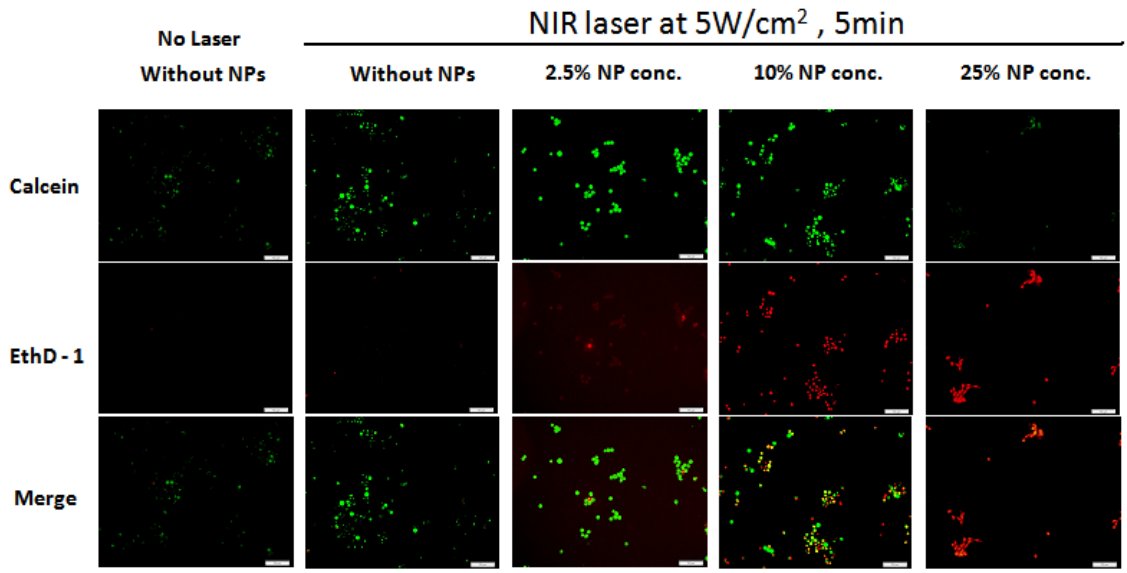

Figure 2.13 Treatment of MCF-7 cells with different concentrations of Au/ CuS nanoparticles and NIR laser at 5W/cm^2 for 5mins. Scale bar: 100 μm

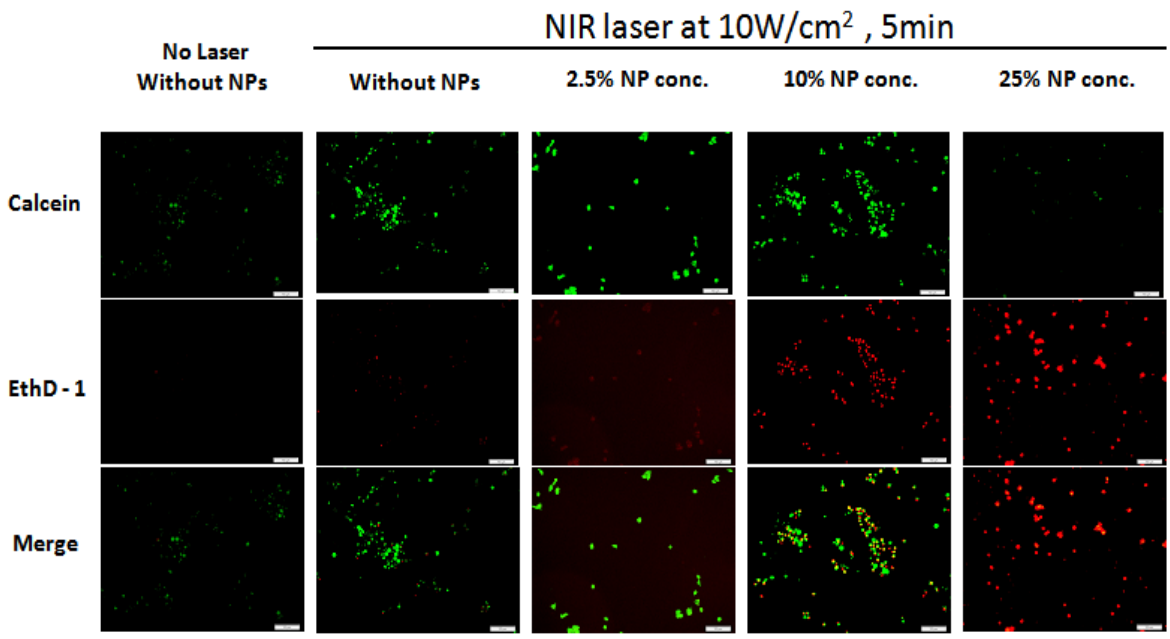

Figure 2.14 Treatment of MCF-7 cells with different concentrations of Au/ CuS nanoparticles and NIR laser at 10W/cm^2 for 5mins. Scale bar: 100 µm

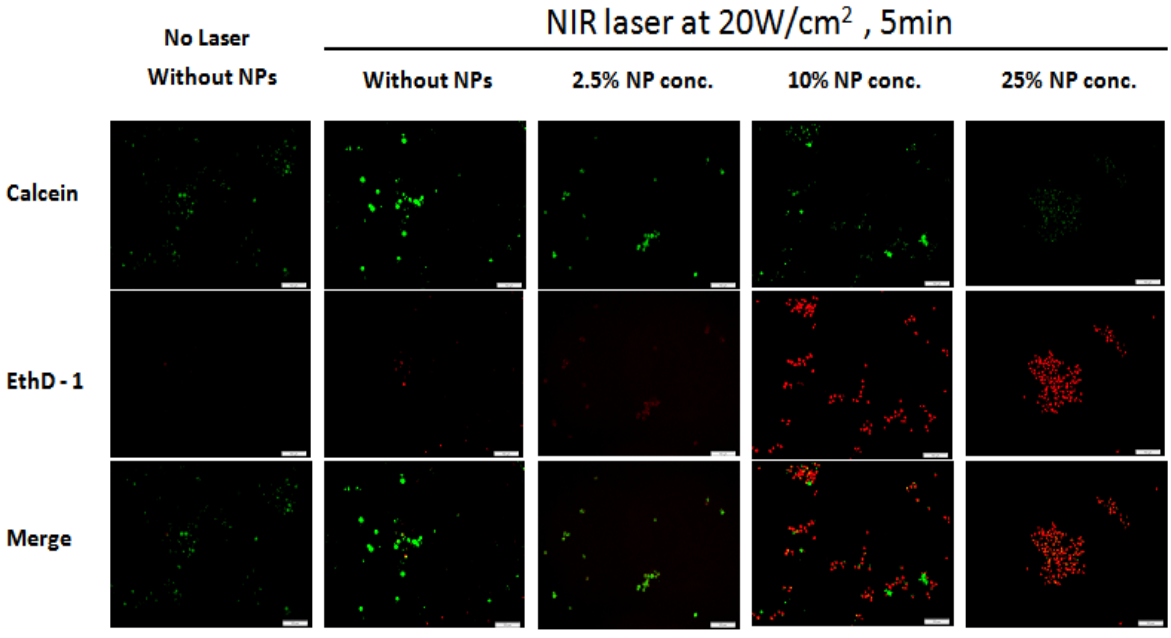

Figure 2.15 Treatment of MCF-7 cells with different concentrations of Au/ CuS nanoparticles and NIR laser at 20W/cm^2 for 5mins. Scale bar: 100 µm

Figures 2.13, 2.14 and 2.15 show the images of living and dead cells after laser treatment at 5, 10 and 20W/cm^2 respectively. The control without nanoparticles and without laser treatment showed no cell death. Even the control without nanoparticles and laser treatment with the three different doses did not show much cell destruction. Only in the presence of nanoparticles cell death was observed. This proved the fact that the laser by itself was not capable of killing the cancer cells (at 5, 10 and 20W/cm^2 laser power) and it was the photothermal conversion ability of Au/ CuS nanoparticles that brought about the destruction of cancer cells.

For 25% concentration of Au/ CuS nanoparticles almost all the cells were destroyed even at 5W/cm^2 of laser power. It has been previously reported that CuS nanoparticles require at least 24 W/cm^2 laser power for 5 mins (from an 808 nm laser) to destroy the cancer cells [30]. Using gold nanorods at least 10 W/cm^2 laser power was required for the HSC and HOC cancer cells to be injured. In our study, a laser power of only 5W/cm^2 was required for the complete destruction of cancer cells. Therefore, it should also be noted that compared with the previous results [30], Au/ CuS nanoparticles afford higher photothermal conversion efficiency at much lower laser irradiation power.

At 10W/cm^2, only 25% concentration of Au/ CuS nanoparticle solution showed complete destruction of cancer cells. For all other concentrations considerable amount of living cells were observed after laser treatment. At a higher laser power of 20 W/cm^2 for 5 min, total cell destruction was observed even at a lower concentration of 10% Au/ CuS.

A quantitive study of photothermal therapy with Au/ CuS nanoparticles was carried out with two different laser output powers (0.125 W/cm^2 and 2 W/cm^2) and three different concentrations (2.5%, 10% and 25% of the original concentration of Au/ CuS). MTT assay was used to determine the cell viability after photothermal treatment. All results are presented as mean ± standard error. Figure 2.16 shows cell viability after 0.125W/cm^2 of NIR laser treatment for 5mins. Though the cell viability decreased with increasing concentration of nanoparticles, the

cell viability still seemed to be more than 80% of that of the control even at the highest (25%) concentration of Au/ CuS used.

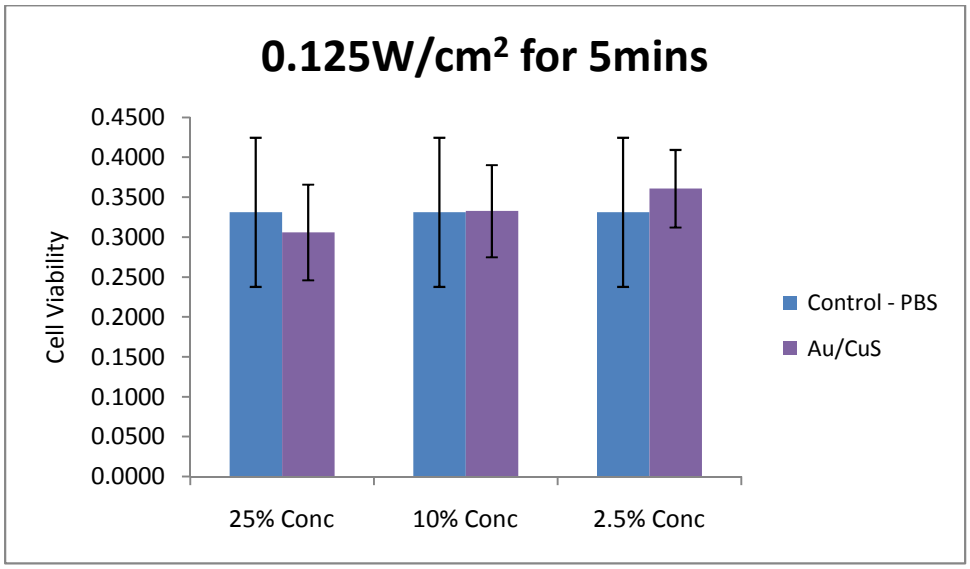

Figure 2.16 Cell viability after 0.125W/cm^2 of NIR laser treatment for 5mins

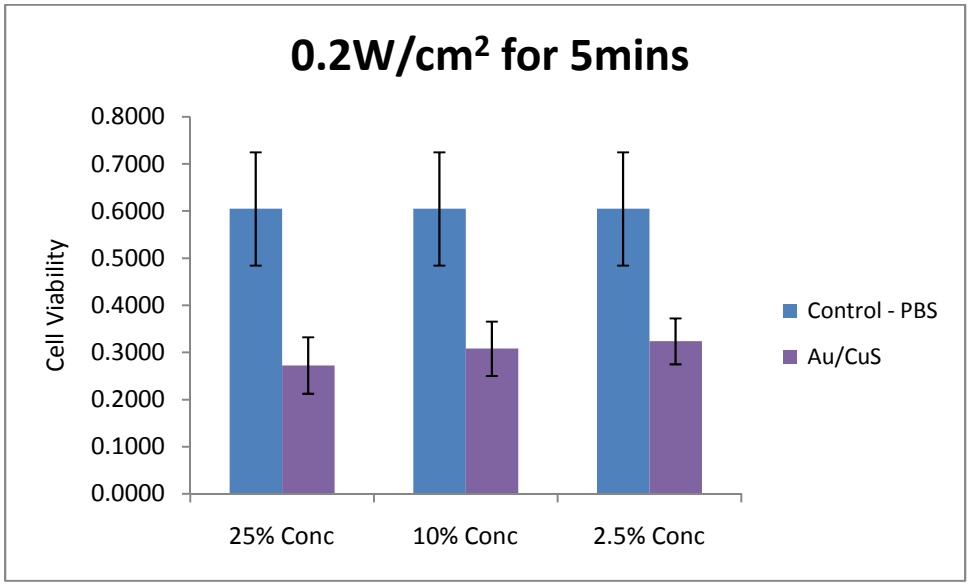

Figure 2.17 Cell viability after 0.2 W/cm^2 of NIR laser treatment for 5mins

Figure 2.17 shows cell viability after 0.2 W/cm^2 of NIR laser treatment for 5mins. Even in this case, the cell viability was observed to decrease with increasing concentration of nanoparticles as a result confirming that Au/ CuS nanoparticles are capable of photothermal therapy. At 0.2 W/cm^2 laser power and 25% concentration of nanoparticles more than 50% of the cancer cells were killed. This laser power is much lower than the safety limit for human skin exposure (~ 0.726 W/cm^2) for a 980nm laser. It is also much lower than the one reported by Qiwei Tian et al. where 0.51 W/cm^2 laser power was used with CuS superstructures for photothermal therapy [37]. But it has no quantitative data showing their cell viability after photothermal treatment. Thus, we can conclude that Au/ CuS nanoparticles are very effective for photothermal therapy even at extremely low laser powers that are safe enough to human skin.

2.4 Conclusion

In this chapter, we have successfully synthesized Au/ CuS nanoparticles and characterized them using several techniques. TEM results confirmed the formation of core/ shell structure of Au/ CuS particles. EDS results confirmed CuS coating on AuNPs. These Au/ CuS nanoparticles have an optical absorption band in the NIR region (maximum absorbance at 981nm) thus making them suitable for in vivo applications. Fluorescence studies demonstrated the formation of metal - ascorbic acid complexes which were responsible for the fluorescence of Au and Au/ CuS nanoparticles. Hence, Au/ CuS nanoparticles were used as fluorescent imaging agents that helped in confirming the nanoparticle uptake by cancer cells. Cellular studies indicated that these nanoparticles are non-toxic and biocompatible. Finally, photothermal studies proved the high photothermal conversion efficiency of Au/ CuS nanoparticles at a laser power much lower than the safety limit for human skin exposure.

In Conclusion, these results demonstrate the great potential of using Au/ CuS nanoparticles for imaging and photothermal ablation of *in vivo* tumor tissues.

CHAPTER 3

PRELIMINARY STUDIES FOR THE INVESTIGATION OF GOLD NANOPARTICLES AS A RADIOSENSITIZER IN AN ORTHOTOPIC HUMAN PROSTATE CANCER RAT MODEL.

3.1 Background

Prostate cancer is the second leading cause of cancer death in American men, behind only lung cancer. Other than skin cancer, prostate cancer is the most common cancer in American men [46]. Radiation therapy is typically delivered 5 days a week for 8 to 9 weeks. Even though this regimen produces excellent treatment outcomes, the length of treatment is neither the most potent biologically, nor the most convenient for the patient. In other disease sites, a fundamental paradigm shift to hypo-fractionated regimens, using stereotactic body radiation therapy, is occurring. However, higher doses of radiation are also accompanied by the increased rate of toxicity to the surrounding normal tissues, such as the rectum and the bladder because there are still unresolved localization uncertainties of the prostate, which are mainly due to 1) daily patient setup error and 2) internal organ motion and deformation before and during treatment [47, 48]. To minimize these uncertainties, physicians may use a rectal balloon for the prostate immobilization,[8] but this method is not ideal because it causes discomfort to the patient. Another method to account for the prostate movement is to add a more margin over the clinical target volume (CTV), which is called a planning target volume (PTV). Consequence of the larger margin causes more exposure to the bladder and the rectum, which may lead to severe complications, such as rectal bleeding [49, 50]. Therefore, the development of new methodologies to selectively target prostate cancer cells through local enhancement of radiation dose while sparing normal tissues is highly desirable.

AuNPs have recently been utilized for both diagnostic and therapeutic purposes. In diagnostic applications, AuNPs are primarily used as contrast agents in modalities including

optical imaging [51, 52], magnetic resonance imaging [53, 54], and computed tomography [55], as well as for molecular probes for specific target detection (i.e. cancer) [54, 56, 57]. AuNPs are also used for delivering and targeting therapeutic agents to a specific site [58-60]. The broad application of AuNPs is attributed to widely tunable properties such as size, shape, composition, as well as ease of surface modification and biocompatibility. In contrast to investigations as imaging contrast agents, AuNPs have not yet actively explored therapeutically, particularly as a dose enhancement agent (radiosensitizer).

It is more than 30 years since the excessive cytotoxicity by high Z radiocontrast agent has been reported after contrast-enhancing imaging [61, 62]. These reports spawned a series the studies of radiosensitizers using high Z materials, such as iodine (Z=53) and gadolinium (Z=64) [61, 63-68]. These studies have been extended to clinical trials in various cancers [69-76]. This dose enhancement effect is primarily derived from the enhanced photoelectric effect, which is approximately proportional to atomic number, Z^3 [77]. In the photoelectric effect, the incident photon ejects an orbital electron, transferring energy in excess of the electron's binding energy to kinetic energy. These secondary electrons are highly ionizing and produce a significant local dose enhancement within a short range (several cell dimensions). In this regard, because the use of gold is highly advantageous as its atomic number (Z=79) is greater than both iodine (Z=53) and gadolinium (Z=64). Below 0.5 MeV, the photoelectric effect is dominant, and the ratio of gold (Z=79) to soft tissue (Z=7.4) is as high as 1217 ($79^3/7.4^3$ at 80.75 keV).

The literatures also support the theoretical dose enhancement from AuNPs. Along with theoretical studies, *in vitro* and *in vivo* studies also have been performed by several research groups. In the *in vitro* experiment performed by Regulla et al, in which cells grown on a thin metallic gold foil were irradiated with filtered x-rays (40-120 kVp), a DEF greater than 100 was reported [79]. In addition to the higher Z value of gold, AuNPs have a unique property of tumor specific extravasation from tumor blood vessels [80, 81]. Typically, tumor vasculature is more

"leaky" compared with normal vasculature. The size of nanoparticles is on the order of the size of "holes" in the tumor blood vessels, making nanoparticles tumor specific. From this property of tumor blood vessels, even pure nanoparticles (without the conjugation of targeting substance) can preferentially reach tumors. Recently, *in vivo* studies using AuNPs have been performed in subcutaneous tumors implanted in mice [45]. In this study, AuNPs 1.9 nm in size were intravenously injected and accumulated in the tumors at concentrations in excess of 0.5% (5 mg Au/g) in weight. From earlier theoretical studies, such a concentration is sufficient to generate a DEF in excess of 2. Though both *in vitro* and *in vivo* subcutaneous studies show a promising treatment effect, the application of AuNPss in radiation therapy has been limited to *in vitro* studies and to *in vivo* irradiation of subcutaneous tumors in small animals. Neither model accurately represents actual tumor biology and physiology, nor would the evaluation of AuNPs activity in a subcutaneous tumor be expected to differ significantly from that in an orthotopic tumor. Therefore, an orthotopic prostate tumor model is highly desirable for the systematic investigation of preclinical environment in this direction. This led us to the investigation of AuNPs as radiosensitizers in an orthotopic human prostate cancer rat model. As a first step towards this goal we have carried out preliminary studies at the in vitro level with gold nanoparticles for radiation enhancement in three different cancer cell lines which will be discussed in this chapter.

3.2 Materials and Methods

3.2.1 Materials

Chloroauric acid ($HAuCl_4$, Aldrich Chemical Company) and Sodium citrate ($C_6H_5Na_3O_7$, Sigma Chemical Company).

3.2.2 Synthesis of AuNPs (nanospheres)

Gold nanospheres with a size of around 40nm were prepared by citrate reduction of chloroauric acid ($HAuCl_4$). Gold nanoparticles of any size can be prepared by changing the ratio between the gold salt and the reducing agent. Firstly, stock solutions of 1 wt % $HAuCl_4$ and 38.8mM sodium citrate were prepared. To 40ml of DI water, 300µl of 1 wt % $HAuCl_4$ solution was added. This solution was then heated on a hot plate while stirring. Once this solution reaches its boiling point, 275µl of 38.8mM sodium citrate solution was added and the heat supply was turned off immediately. In a few minutes we can see the solution color changing from dark blue to red indicating the formation of AuNPs. These nanoparticles were washed several times and centrifuged to increase their concentration by two.

3.2.3 Characterization of AuNPs

The synthesized nanoparticles were characterized by HRSEM (Hitachi S-5000H), Dynamic light scattering (Zeta potential analyzer - Brookhaven Instruments) and UV-Vis spectroscopy (Shimadzu UV-2450).

3.2.4 Cell culture and Nanoparticle incubation

For in vitro radiation enhancement studies three different cell lines were used. The three different cell lines used are HeLa, LNCap, and DU145. HeLa cells are derived from cervical cancer cells. LNCap, and DU145 are prostate cancer cell lines.

Cell culture: The cancer cells were washed 3 times with PBS (37ºC) followed by replacement with medium. The cells were then seeded on a glass cover slip overnight keeping it in a 35 mm dish. This was preferably done for 24 hrs at 37℃ and 5% CO_2.

Nanoparticle treatment: The cultured cells were incubated with AuNPs for 24 hours (unless mentioned) at 37℃ and 5% CO_2.

3.2.5 Radiation Sources

Radiation treatment was carried out using Gulmay D3225 orthovoltage unit in our experiments.

3.2.6 γ-H2AX Indirect Immunofluorescence Assay

After radiation treatment, the cells were again placed in a 37℃ and 5% CO_2 incubator. Cell fixing was done at required time points and analyzed by indirect immunofluorescence. Cells were fixed with freshly prepared 4% paraformaldehyde (1ml for 35mm dish) 20 min. Cover slips were washed three times with PBS, and the cells were permeabilized with 0.5% Triton X-100 (1 ml for a 35 mm dish) for 1 hour at room temperature. The cells were then blocked with the blocking buffer for minimum 1 hr at room temperature and then incubated with the appropriate antibodies diluted in 3% BSA overnight at 4℃. The antibody used for these in vitro γH2AX studies was mouse monoclonal. After primary incubation cover slips were then washed three times with PBS and secondary antibody (mousered) was incubated for 1 hour at room temperature in the dark. They were again washed three times with PBS and the samples were kept moist. The cell nuclei were then stained with 6-diamidino-2-phenylindole (DAPI) for 10 min followed by washing three times with PBS. The cover slips were mounted onto 1-mm glass microscope slides with Vectashield antifade. The cells were imaged using a fluorescence microscope.

3.2.7 Sectional and 3D imaging

Phalloidin staining was done for 3D and sectional imaging. After washing the secondary antibody with PBS three times, phalloidin was added and incubated for 30 mins. It was then washed lightly and mounted with DAPI for fluorescence imaging.

3.2.8 Statistical Analysis

All results are presented as mean ± SE (standard error). Results are analyzed using Student t-test, with $p < 0.05$ considered to be statistically significant.

3.3 Results and Discussion

3.3.1 Size, shape and uniformity of nanoparticles

3.3.1.1 HRSEM

AuNPs observed under a high resolution SEM are shown in figures 3.1 and 3.2. The AuNPs appeared to be are very uniform in size and spherical in shape. Their size was around 45 nm in diameter which is the size we desire for our experiments in radiation therapy. It has been earlier reported that AuNPss of size close to 50nm have a better cellular uptake thus helping in the enhancement of radiation effects [42].

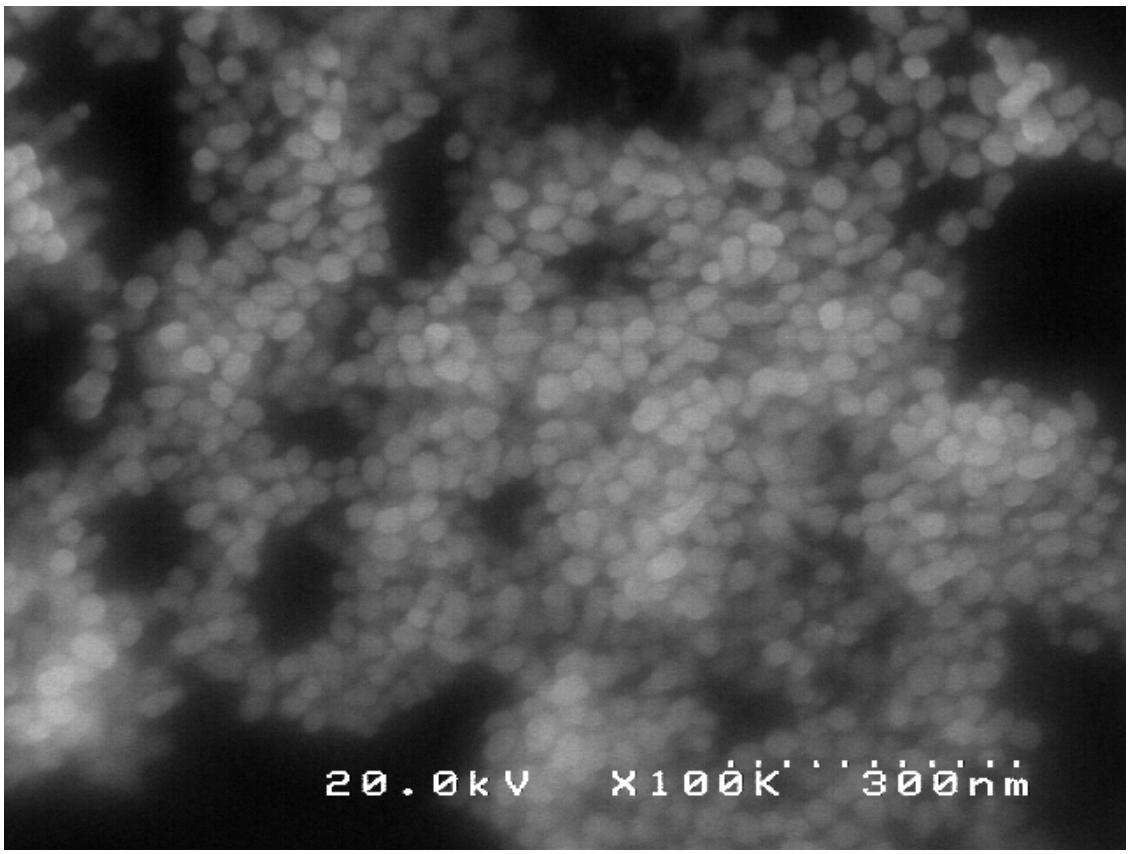

Figure 3.1 HRSEM of AuNPs (lower magnification)

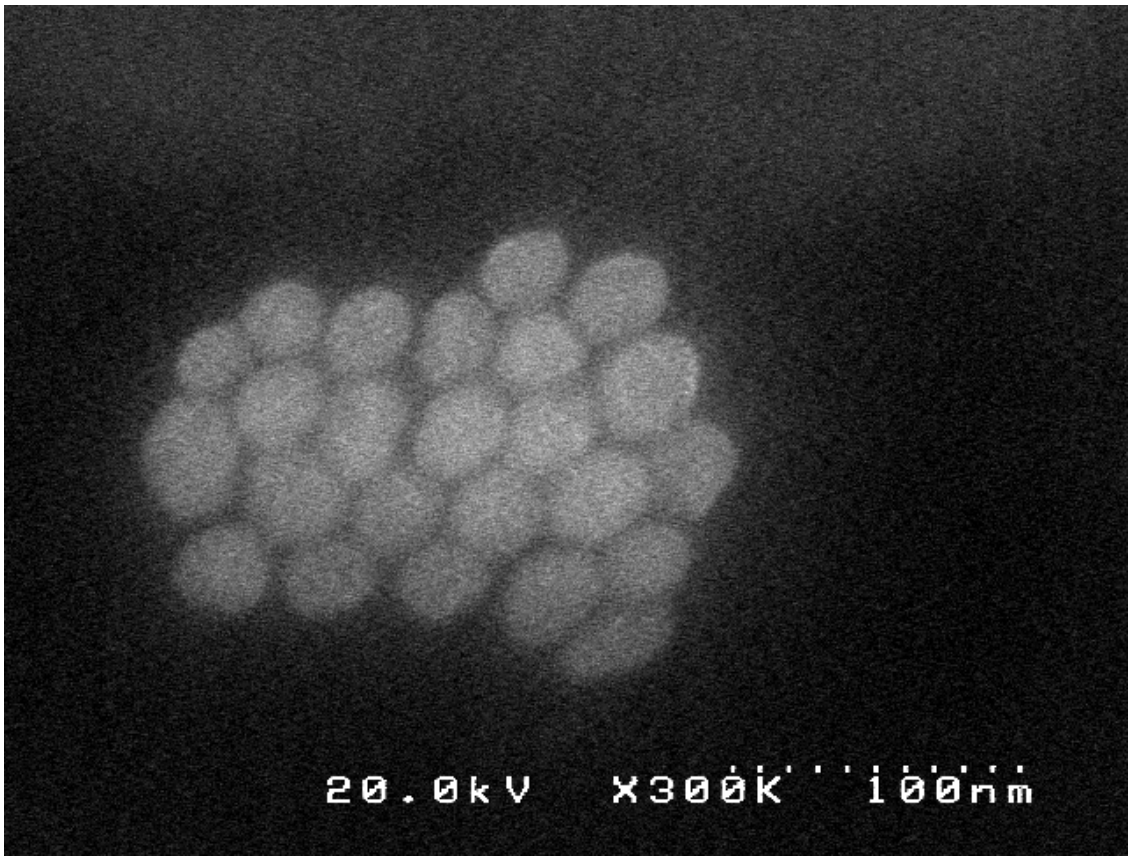

Figure 3.2 HRSEM of AuNPs (higher magnification)

3.3.1.2 UV-Vis Spectroscopy

Figure 3.3 shows the absorption spectrum of AuNPs. The maximum absorption was at 530 nm wavelength. This matched with literatures which stated that gold nanospheres display a single absorption peak in the visible range between 510 nm and 550 nm [1]. Wolfgang et al. reported the size determination of uncoated gold nanospheres from UV-Vis Spectra. From their paper it was obtained that for a maximum absorption wavelength of 530.4 nm the diameter of the gold nanospheres would be around 48 nm. This agreed with our HRSEM result of 45 nm, thereby confirming the size of our AuNPs.

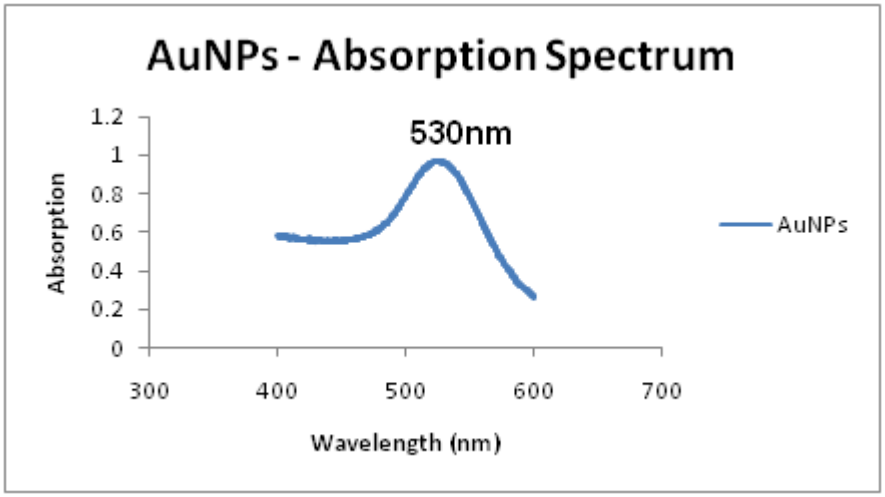

Figure 3.3 Absorption spectrum of AuNPs

3.3.1.3 Dynamic Light Scattering

Figure 3.4 gives the size distribution of AuNPs. Most of the nanoparticles were observed to be around 48nm in size which agrees with our previous HRSEM and UV-Vis results. From DLS measurements we also obtained the average diameter to be 39.985 nm which is as well close to our previous results. For an average of 40 nm, these AuNPs had a relative variance of only 0.2 which proves that they are almost uniform in size.

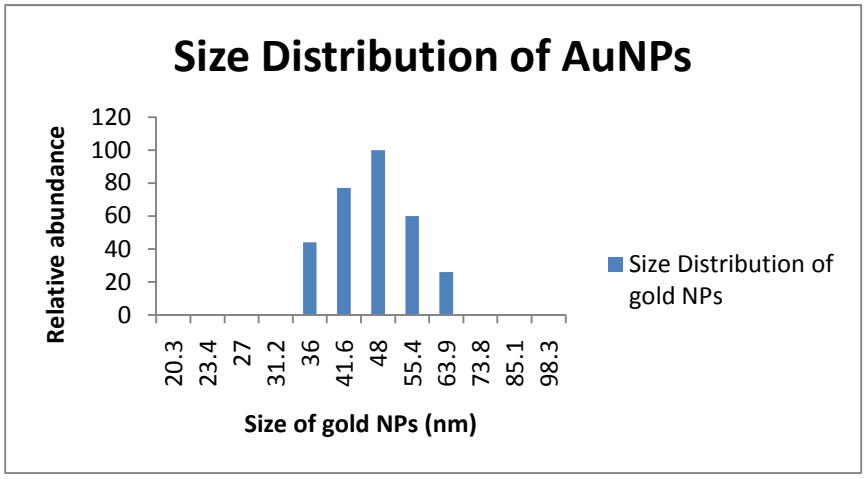

Figure 3.4 Size distribution of AuNPs

Thus from the above characterization techniques we get that these AuNPs are 45 nm in diameter, spherical in shape and uniform in size.

3.3.2. Radiation enhancement in HeLa cells with AuNPs

HeLa is the oldest and most regularly used human cell line. The line was derived from cervical cancer cells. HeLa cell line was found to be extremely durable and prolific. Phosphorylated histone H2AX (γH2AX) serves as a biomarker for formation of DNA double-strand break repair complexes.

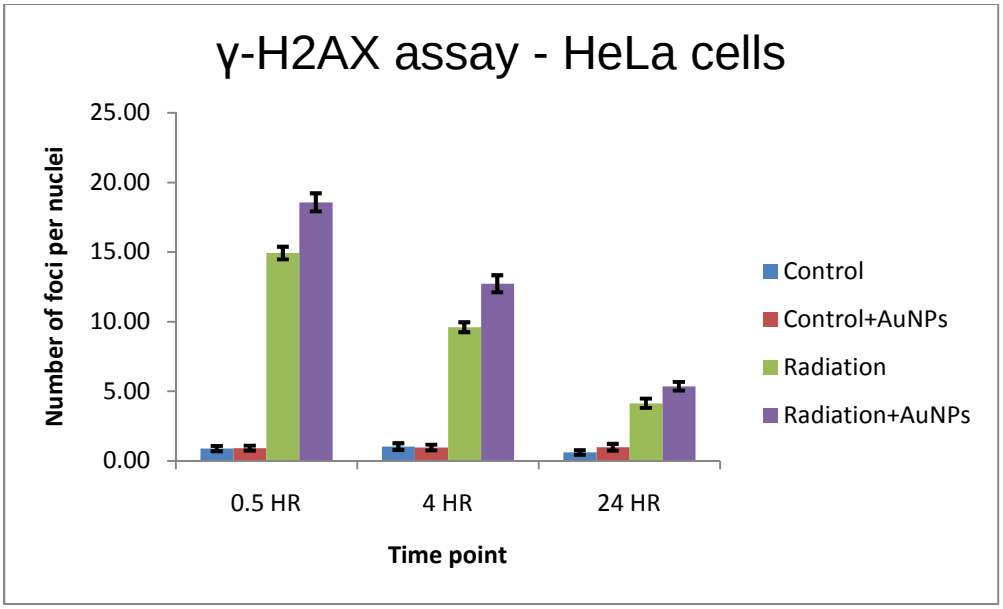

Figure 3.5 Comparison of radiation enhancement in HeLa cells with AuNPs at different time points after radiation treatment

Figure 3.5 shows the radiation dose enhancement in HeLa cells with AuNPs at 2Gy and 225 kVp x-ray radiation. After 0.5 hour of irradiation of HeLa cells, the DNA damage is around 25% more for radiation + AuNPs than radiation only. This shows that there is radiation enhancement due to AuNPs. The more the damage to DNA the more are the chances of cell death. Even after 4 hours of irradiation the DNA damage for radiation + AuNPs was ~ 33% higher than radiation only. After 24 hours there was still an enhancement of ~40% in the

radiation dose with AuNPs. The results from control and control + AuNPs were similar showing almost no DNA damage.

3.3.3 Radiation enhancement in LNCap cells with AuNPs

LNCaP cells are androgen-sensitive human prostate adenocarcinoma cells. They are adherent epithelial cells growing in aggregates and as single cells. Figure 3.6 gives the radiation dose enhancement in LNCap cells with AuNPs at 1Gy dose and 105 kVp x-ray radiation. Only 19% dose enhancement (with AuNPs) was observed after 0.5 hours and 17% after 4 hours of irradiation with AuNPs. But after 24 hours of treatment 69% dose enhancement was observed for radiation + AuNPs. Almost no DNA damage was observed for control and control + AuNPs at different time points.

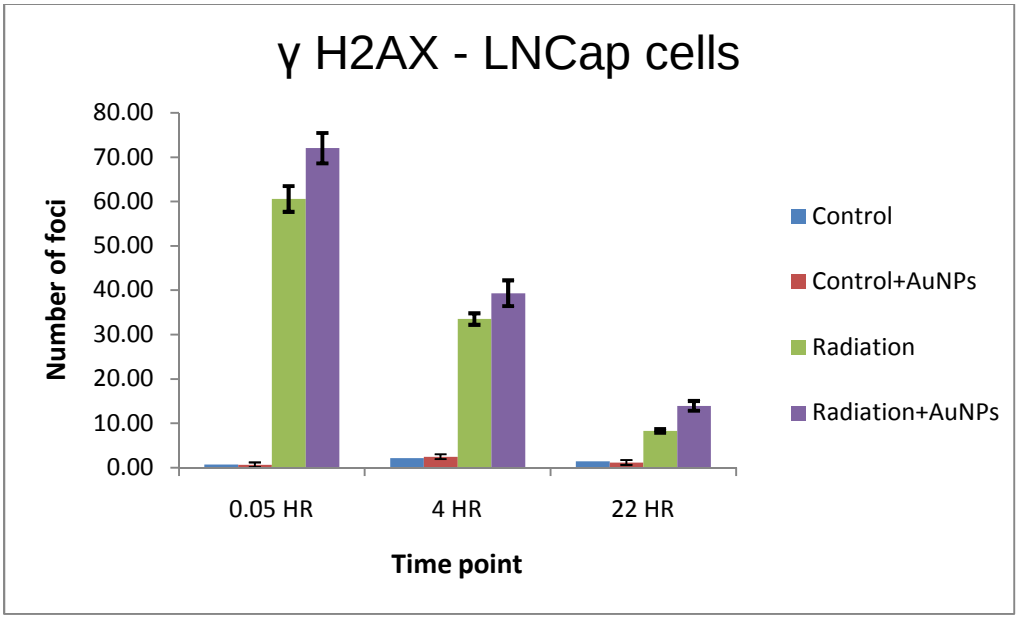

Figure 3.6 Comparison of Radiation enhancement in LNCap cells with AuNPs at different time points after radiation treatment

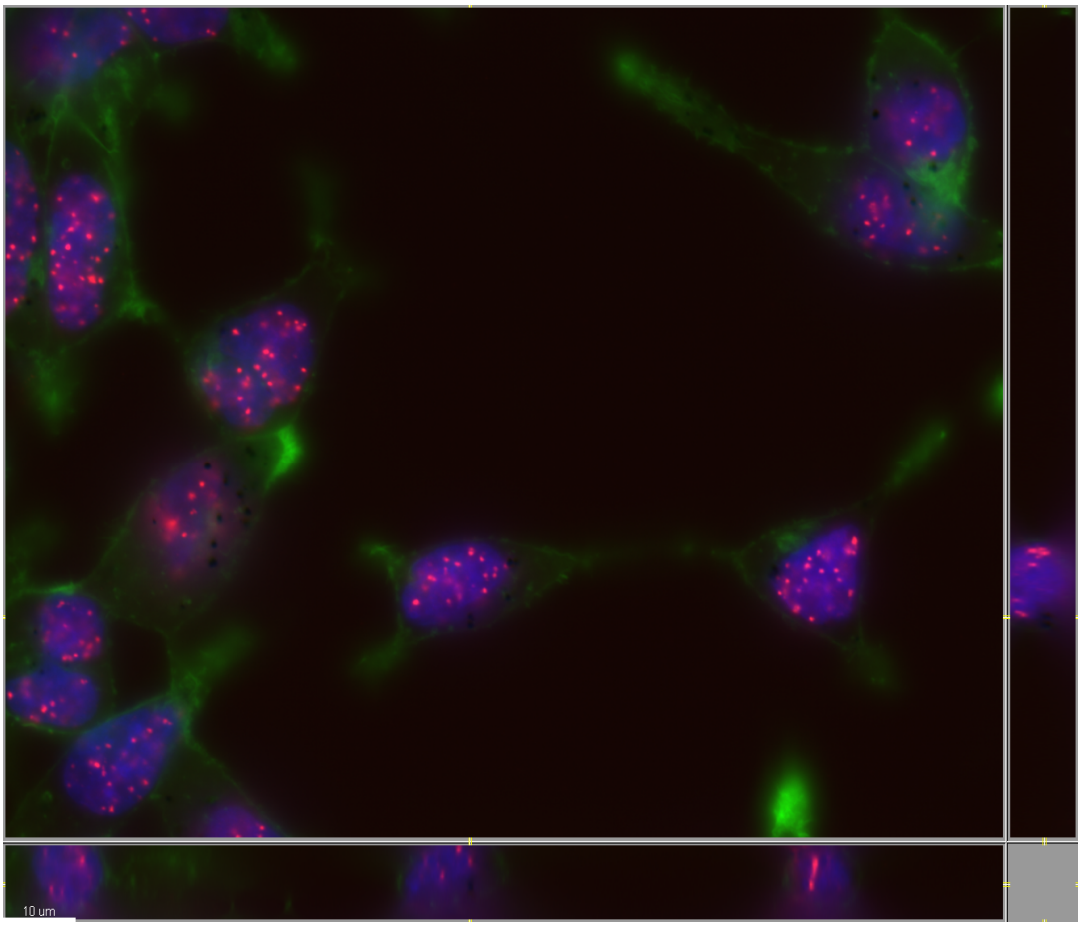

Figure 3.7 Sectional image showing DNA double-strand breaks in LNCap cells after irradiation with AuNPs

Figure 3.7 and 3.8 clearly show DNA double strand break in LNCap cells after irradiation with AuNPs. Phosphorylated histone H2AX (γH2AX) serves as a biomarker for formation of DNA double-strand break repair complexes. Red shows H2AX foci, the nuclei are stained blue with DAPI and Phalloidin stains the actin filaments in the cells shown in green. Black spots were observed in the cells which we expect to be clusters of AuNPs. Unfortunately, there is no scientific evidence for this, but upon comparison with the control group (radiation only group) we can say that these black dots could be AuNPs. As AuNPs absorb most of light, Phalloidin staining (green fluorescence) does not show up in the place where nanoparticles are present. This is what we call negative contrast.

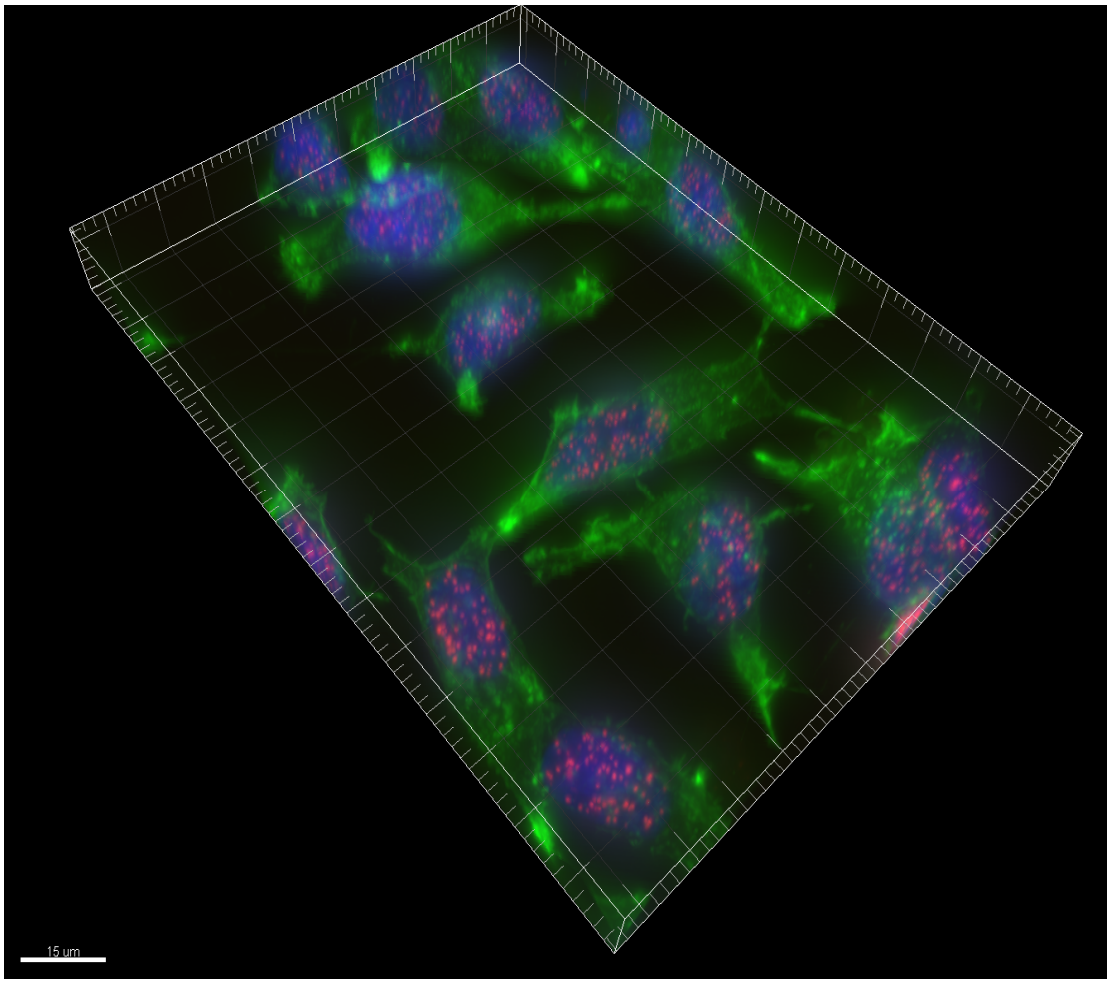

Figure 3.8 3D image showing DNA double-strand breaks in LNCap cells after irradiation with AuNPs

Radiation produces ions, radicals and free electrons, as they travel through matter. The electrons in turn generate large quantities of a second generation of radicals, ions and free electrons that interact with DNA inside living cells causing enough damage that could lead to cell death. To understand the mechanism behind enhanced sensitization properties of AuNPs, Carter et al. performed Monte Carlo calculations and pointed out that the cause for this phenomenon could be a combination of the following effects: (1) enhanced localized absorption of X-rays by nanostructures; (2) effective release of low-energy electrons from AuNPs; and (3) efficient deposition of energy in water in the form of radicals and electrons. However this is only

when AuNPs are in close proximity to DNA. The exact mechanisms of cell damage when GNPs are localized away from DNA (either when they are in the media or in the cytoplasm of the cell) are not known yet [24].

From sectional and 3D image, the morphology of LNCap cells seemed to be more spiked than rounded. Our hypothesis is that the cell morphology could be one of the factors that affect radiation enhancement. Since they have a spiked morphology even if the nanoparticles are uptaken by the cells it is not necessary that they will be close enough to the nucleus to cause the DNA damage. As reported previously nothing much is known about the mechanism of cell damage when AuNPs are localized away from the nucleus (in the media or in the cytoplasm of the cell). For these reasons we tried similar experiments with DU145 cell line, which has a more rounded morphology, to see if there is comparatively more DNA damage.

3.3.4 Radiation enhancement in DU145 cells with AuNPs

DU145 cell line is a "classical" cell line of prostatic cancer. DU145 cells have moderate metastatic potential compared to PC3 cells which have high metastatic potential. With DU145 cell line we obtained some interesting results. Figure 3.9 shows radiation dose enhancement in DU145 cells with AuNPs for different radiation doses (1Gy, 2Gy and 4Gy) and energies (225kVp and 105kVp). At 1 Gy there is no significant increase in DNA damage for radiation + AuNPs at both the energies of 105 and 225 kVp. At 2 Gy there is significant radiation enhancement at both the energies of 105 and 225 kVp. More that 50% radiation enhancement was observed at 225 kVp and 35% enhancement at 105 kVp. Thus, upon comparing the radiation enhancement between the two energies (105 and 225 kVp) at 2Gy we get that the radiation enhancement is more at 225 kVp than at 105 kVp radiation energy. This is actually not in agreement with a previously reported work where they say that we can expect a decrease in radiation enhancement at higher energies [41]. But it is too early to make a statement as these are just preliminary studies and more studies need to be done. At 4Gy there is no significant radiation enhancement at the respective energies of 105 and 225 kVp.

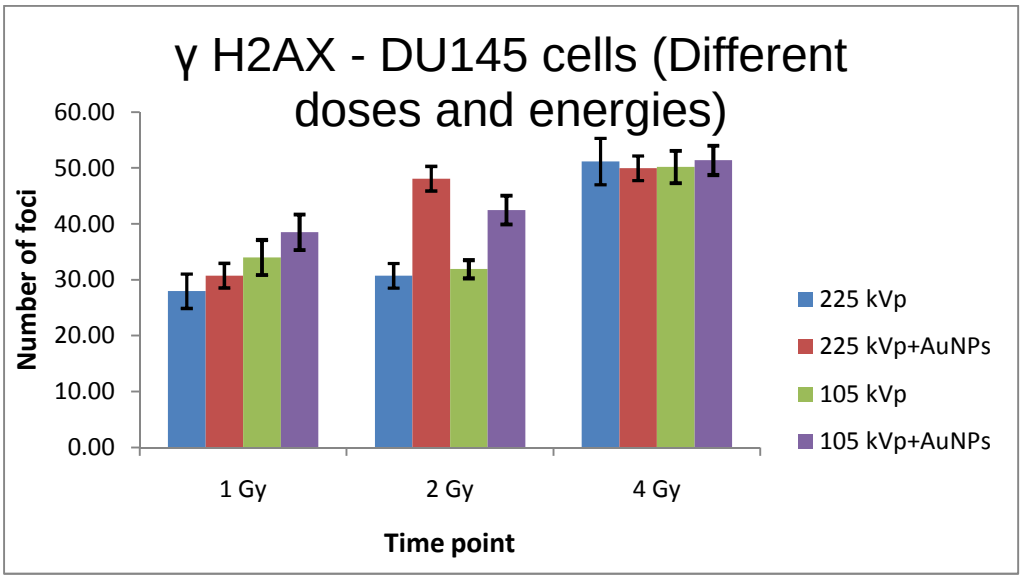

Figure 3.9 Comparison of radiation enhancement in DU145 cells with AuNPs for different radiation doses and energies

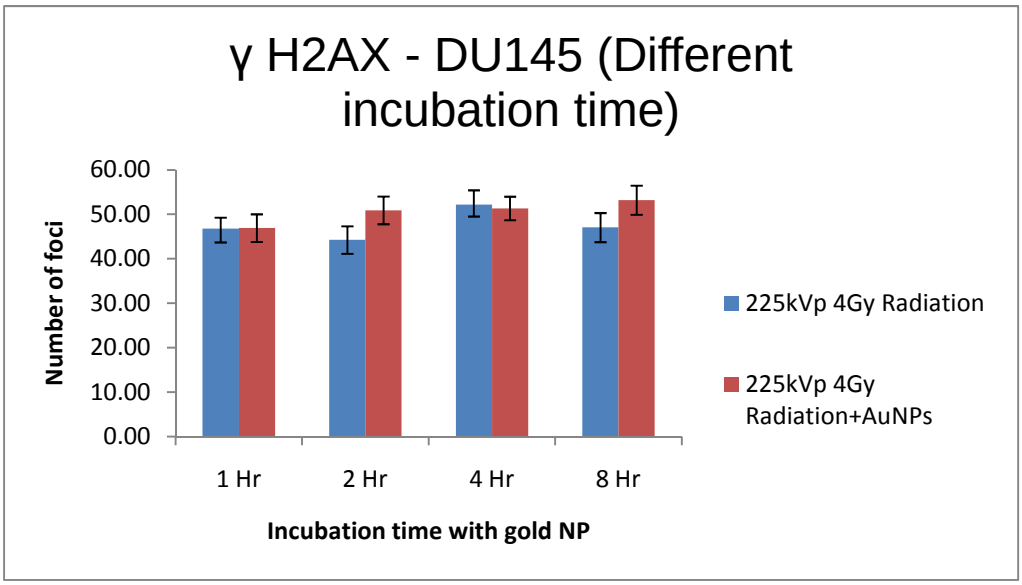

Figure 3.10 Radiation enhancement in DU145 cells with AuNPs for different incubation time

Figure 3.10 shows radiation enhancement in DU145 cells for different incubation time (1hr, 2hr, 4hr and 8hr) with AuNPs. The radiation dose used was 4Gy and radiation energy was

225kVp. These measurements were taken after 4 hours of irradiation and we could not see any significant radiation enhancement with the different incubation times.

3.4 Conclusion

In this chapter, we successfully synthesized AuNPs and used it for the enhancement of radiation effects in prostate cancer cells. Preliminary studies at the in vitro level for radiation enhancement with AuNPs are reported. Radiation enhancement in three different cell lines was studied. The three different cell lines showed different radiation enhancement effects upon irradiation with AuNPs.

CHAPTER 4

SUMMARY AND FUTURE WORK

In the work presented, we successfully developed Au and Au/ CuS nanoparticles for application in Cancer therapy.

The Au/ CuS nanoparticles were effectively used for photothermal therapy and imaging. These nanoparticles had better photothermal conversion efficiency than only gold or only CuS nanoparticle systems for photothermal therapy. TEM, EDS and UV-Vis-NIR results confirmed the CuS coating on AuNPs. From UV-Vis-NIR spectroscopy we obtained that these core/shell nanoparticles have maximum absorbance at 981 nm and absorption intensity much higher than only gold and only CuS nanoparticles systems. This, in turn attributed to their relatively high photothermal conversion efficiency. The most important advantage of having an optical absorption band in the NIR region is that it makes them suitable for in vivo applications. The Au/ CuS nanoparticles were also seen to be fluorescent. From fluorescence studies we hypothesized that their fluorescence could be due to the formation of metal - ascorbic acid complexes in the solution. Hence, Au/ CuS nanoparticles were used as fluorescent imaging agents that helped in confirming the nanoparticle uptake by cancer cells. Cellular studies indicated that these nanoparticles are non-toxic and biocompatible. Finally, photothermal studies proved the high photothermal conversion efficiency of Au/ CuS nanoparticles at much lower laser irradiation power of 0.2 W/cm^2. This laser power is much lesser than the safety limit for human skin exposure of ~ 0.726 W/cm^2 for a 980nm laser. Thus, these results demonstrate the great potential of using Au/ CuS nanoparticles in imaging and photothermal ablation of *in vivo* tumor tissues. Future work for this project would include the targeting of Au/ CuS nanoparticles for even higher photothermal conversion efficiency to be used in in vivo studies for selective photothermal therapy.

Another research work was carried out with AuNPs which were used for radiation enhancement in cancer cells at the in vitro level. As a first step towards the investigation of AuNPs as radiosensitizers in an orthotopic human prostate cancer rat model, preliminary studies were carried out at the in vitro level. Radiation enhancements in three different cell lines (HeLa, LNCap and DU145) were studied. All the three cell lines showed different radiation enhancement effects upon irradiation with AuNPs. Future work in this project would be to functionalize the AuNPs with targeting ligands and improve the efficiency of radiation enhancement so that in vivo studies can be carried out in an orthotopic human prostate cancer rat model.

REFERENCES

1. Weibo Cai, Ting Gao, Hao Hong, Jiangtao Sun. Applications of gold nanoparticles in cancer Nanotechnology. Nanotechnology, Science and Applications 2008:1 17–32.
2. Health Scout: Tumor Definition and Causes. Available from: http://www.healthscout.com/ency/1/001310.html
3. Lisa Brannon-Peppas, James O. Blanchette. Nanoparticle and targeted systems for cancer therapy. Advanced Drug Delivery Reviews 56 (2004) 1649– 1659.
4. G.D. Grossfeld, P.R. Carrol, N. Lindeman, Thrombospondin-1 expression in patients with pathologic state T3 prostate cancer undergoing radical prostatectomy: association with p53 alterations, tumor angiogenesis and tumor progression, Urology 59 (2002) 97– 102.
5. A. Jones, A.L. Harris, New developments in angiogenesis: a major mechanism for tumor growth and target for therapy, Cancer Journal from Scientific American 4 (1998) 209– 217
6. American cancer Society: Surgery. Available from: http://www.cancer.org/acs/groups/cid/documents/webcontent/003022-pdf.pdf
7. National Cancer Institute – Radiation Therapy. Available from: http://www.cancer.gov/cancertopics/factsheet/Therapy/radiation
8. NIH Medline Plus. Available from: http://www.nlm.nih.gov/medlineplus/magazine/issues/spring09/articles/spring09pg7-8.html
9. National Cancer Institute: Cancer Topics: Prostrate Cancer Treatment. Available from: http://www.cancer.gov/cancertopics/pdq/treatment/prostate/Patient/page4
10. Xiaohua Huang, Mostafa A. El-Sayed. Gold nanoparticles: Optical properties and implementations in cancer diagnosis and photothermal therapy. Journal of Advanced Research (2010) 1, 13–28.

11. Chitta Ranjan Patra, Resham Bhattacharya, Debabrata Mukhopadhya, Priyabrata Mukherjee. Fabrication of gold nanoparticles for targeted therapy in pancreatic cancer. Advanced Drug Delivery Reviews 62 (2010) 346–361.
12. Katz, E. and I. Willner. Integrated nanoparticle-biomolecule hybrid systems: Synthesis, properties, and applications. Angewandte Chemie-International Edition, 2004. 43(45): p. 6042.
13. Elodie Boisselier and Didier Astruc. Gold nanoparticles in nanomedicine: preparations, imaging, diagnostics, therapies and toxicity. Chem. Soc. Rev., 2009, 38, 1759–1782.
14. Simon P Fricker. Medical Uses of Gold Compounds: Past, Present and Future. Gold Bulletin 1996, 29(2), 53-60.
15. P. Baptista, G. Doria , P. Quaresma. Gold nanoparticles for the development of clinical diagnosis methods. Anal Bioanal Chem (2008) 391:943–950.
16. Prashant K. Jain, Ivan H. El-Sayed, Mostafa A. El-Sayed. Au nanoparticles target cancer. Nanotoday (Feb 2007) Vol. 2, Number 1, 18-29.
17. American Chemical Society: Radiation side effects. Available from: http://www.cancer.org/Treatment/TreatmentsandSideEffects/TreatmentTypes/Radiation/RadiationTherapyPrinciples/radiation-therapy-principles-radiation-side-effects
18. American Society of clinical Oncology - Surgery Side effects. Available from: http://www.cancer.net/patient/All+About+Cancer/Cancer.Net+Feature+Articles/Side+Effects/Side+Effects+of+Cancer+Surgery
19. American Society of clinical Oncology – Chemotherapy. Available from: http://www.cancer.net/patient/All+About+Cancer/Cancer.Net+Feature+Articles/Side+Effects/Side+Effects+of+Chemotherapy
20. Kioskea Health-Cancer Side Effects. Available from: http://health.kioskea.net/contents/cancer/05_les-traitements-du-cancer.php3
21. Health matters inside – Immunotherapy http://www.healthmattersinside.com/immunotherapy-side-effects/

22. Prakash Rai, Srivallesha Mallidi, Xiang Zheng, Ramtin Rahmanzadeh, Youssef Mir, Stefan Elrington, Ahmat Khurshid, Tayyaba Hasan. Development and applications of photo-triggered theranostic agents, Adv. Drug Deliv. Rev. (2010), doi:10.1016/j.addr.2010.09.002.
23. Partha Ghosh, Gang Han, Mrinmoy De, Chae Kyu Kim, Vincent M. Rotello. Gold nanoparticles in delivery applications. Advanced Drug Delivery Reviews 60 (2008) 1307–1315.
24. Salomeh Jelveh and Devika B. Chithrani. Gold Nanostructures as a Platform for Combinational Therapy in Future Cancer Therapeutics, *Cancers (*2011), *3*, 1081-1110.
25. Ivan H. El-Sayed, Xiaohua Huang, Mostafa A. El-Sayed. Selective laser photo-thermal therapy of epithelial carcinoma using anti-EGFR antibody conjugated gold nanoparticles. Cancer Lett. (2006) 239, 129.
26. Urbanska K, Romanowska-Dixon B, Matuszak Z, Oszajca J, Nowak-Sliwinska P, Stochel G. Indocyanine green as a prospective sensitizer for photodynamic therapy of melanomas. Acta Biochim Pol. 2002; 49(2):387-91.
27. X. Huang, P.K. Jain, I.H. El-Sayed, M.A. El-Sayed. Determination of the minimum temperature required for selective photothermal destruction of cancer cells with the use of immunotargeted gold nanoparticles. *Photochem. Photobiol.*2006, 82 (2), 412-417.
28. Stephan Link and Mostafa A. El-Sayed. Spectral Properties and Relaxation Dynamics of Surface Plasmon Electronic Oscillations in Gold and Silver Nanodots and Nanorods. *J. Phys. Chem. B* (1999) 103, 8410
29. Stephan Link and Mostafa A. El-Sayed. Optical properties and ultrafast dynamics Of Metallic Nanocrystals. Annu. Rev. Phys. Chem. 2003. 54:331–66.
30. Yuebin Li, Wei Lu, Qian Huang, Chun Li and Wei Chen. Copper sulfide nanoparticles for photothermal ablation of tumor cells. Nanomedicine (2010) 5(8), 1161–1171.
31. Balzani V, Carassiti V: Photochemistry of Coordination Compounds. Academic Press, London, UK (1970).

32. Zhenhua Sun, Zhi Yang, Jianhua Zhou, Man Hau Yeung, Weihai Ni, Hongkai Wu, and Jianfang Wang. A General Approach to the Synthesis of Gold–Metal Sulfide Core–Shell and Heterostructures. Angew. Chem. 2009, 121, 2925 –2929.
33. Babak Nikoobakht and Mostafa A. El-Sayed. Preparation and Growth Mechanism of Gold Nanorods (NRs) Using Seed-Mediated Growth Method. Chem. Mater. 2003, 15, 1957-1962.
34. Xu HL, Wang WZ, Zhu W. Sonochemical synthesis of crystalline CuS nanoplates via an *in situ* template route. *Mat. Lett.* 60, 2203–2206 (2006).
35. Zhu HL, Ji X, Yang D, Ji Y, Zhang H. Novel CuS hollow spheres fabricated by a novel hydrothermal method. *Microporous Mesoporous Mater.* 80, 153–156 (2005).
36. Lauren Wintzinger, Wei An, C. Heath Turner, Ph.D., * Yuping Bao, Ph.D. Synthesis and Modeling of Fluorescent Gold Nanoclusters. JOSHUA, May 2010, Vol 7, 24-27.
37. Qiwei Tian, Minghua Tang, Yangang Sun, Rujia Zou, Zhigang Chen, Meifang Zhu, Shiping Yang, Jinglong Wang, Jianhua Wang and Junqing Hu. Hydrophilic Flower-Like CuS Superstructures as an efficient 980 nm Laser-Driven Photothermal Agent for Ablation of Cancer Cells. Adv. Mater. 2011, 23, 3542–3547.
38. M. Zhou, R. Zhang, M. A. Huang, W. Lu, S. L. Song, M. P. Melancon, M. Tian, D. Liang, C.Li. A Chelator-Free Multifunctional [^{64} Cu] CuS Nanoparticle Platform for Simultaneous Micro-PET/CT Imaging and Photothermal Ablation Therapy. J. Am. Chem. Soc. 2010, 132, 15351.
39. Chatterjee, A.; Magee J.L. Theoretical investigation of the production of strand breaks in DNA by water radicals. *Radiat. Prot. Dosim.* 1985, *13*, 137-140.
40. Boudaiffa B.; Cloutier P.; Hunting D.; Huels M.A.; Sanche L. Resonant formation of DNA strand breaks by low-energy (3 to 20 ev) electrons. *Science* 2000, *287*, 1658-1660.
41. Chithrani, B.D.; Jelveh, S.; Jalali, F.; Van Prooijen, M.; Allen, C.; Bristow, R.G.; Hill, R.P.; Jaffray, D.A. Gold nanoparticles as a radiation sensitizer in cancer therapy. *Radiat. Res.* 2010, *173*, 719-728.

42. Chithrani, B.D.; Ghazani, A.A.; Chan, W.C.W. Determining the size and shape dependence of gold nanoparticle uptake into mammalian cells. *Nano Lett.* 2006, *6*, 662-668.
43. Greish, K. Enhanced permeability and retention of macromolecular drugs in solid tumors: A royal gate for targeted anticancer nanomedicines. *J. Drug Target* 2007, *15*, 457-464.
44. Choi, C.H.J.; Alabi, C.A.; Webster, P.; Davis, M.E. Mechanism of active targeting in solid tumors with transferrin-containing gold nanoparticles. *Proc. Natl. Acad. Sci. USA* 2010, *107*, 1235-1240.
45. James F. Hainfeld, F. Avraham Dilmanian, Daniel N. Slatkin and Henry M. Smilowitz. Radiotherapy enhancement with gold nanoparticles. JPP 2008, 60: 977–985.
46. Prostate Cancer Statistics. Available from: http://www.cancer.org/Cancer/ProstateCancer/DetailedGuide/prostate-cancer-key-statistics
47. Rudat V, Schraube P, Oetzel D, Zierhut D, Flentje M, Wannenmacher M. Combined error of patient positioning variability and prostate motion uncertainty in 3D conformal radiotherapy of localized prostate cancer. *Int J Radiat Oncol Biol Phys,* vol. 35, pp. 1027-34, Jul 15 1996.
48. Wu J, Haycocks T, Alasti H, Ottewell G, Middlemiss N, Abdolell M, Warde P, Toi A, Catton C. Positioning errors and prostate motion during conformal prostate radiotherapy using on-line isocentre set-up verification and implanted prostate markers. *Radiother Oncol,* vol. 61, pp. 127-33, Nov 2001.
49. Pollack A, Zagars GK, Starkschall G, Antolak JA, Lee JJ, Huang E, von Eschenbach AC, Kuban DA, Rosen I. Prostate cancer radiation dose response: results of the M. D. Anderson phase III randomized trial. *Int J Radiat Oncol Biol Phys,* vol. 53, pp. 1097-105, Aug 1 2002.
50. Boersma LJ, van den Brink M, Bruce AM, Shouman T, Gras L, te Velde A, Lebesque JV. Estimation of the incidence of late bladder and rectum complications after high-dose (70-78 GY) conformal radiotherapy for prostate cancer, using dose-volume histograms. *Int J Radiat Oncol Biol Phys,* vol. 41, pp. 83-92, Apr 1 1998.

51. K. H. Song*, et al.*, "Near-infrared gold nanocages as a new class of tracers for photoacoustic sentinel lymph node mapping on a rat model," *Nano Lett,* vol. 9, pp. 183-8, Jan 2009.
52. K. H. Song*, et al.*, "Noninvasive in vivo spectroscopic nanorod-contrast photoacoustic mapping of sentinel lymph nodes," *Eur J Radiol,* vol. 70, pp. 227-31, May 2009.
53. M. F. Kircher*, et al.*, "A multimodal nanoparticle for preoperative magnetic resonance imaging and intraoperative optical brain tumor delineation," *Cancer Res,* vol. 63, pp. 8122-5, Dec 1 2003.
54. S. A. Anderson*, et al.*, "Magnetic resonance contrast enhancement of neovasculature with alpha(v)beta(3)-targeted nanoparticles," *Magn Reson Med,* vol. 44, pp. 433-9, Sep 2000.
55. D. Kim*, et al.*, "Antibiofouling polymer-coated gold nanoparticles as a contrast agent for in vivo X-ray computed tomography imaging," *J Am Chem Soc,* vol. 129, pp. 7661-5, Jun 20 2007.
56. P. M. Winter*, et al.*, "Molecular imaging of angiogenesis in early-stage atherosclerosis with alpha(v)beta3-integrin-targeted nanoparticles," *Circulation,* vol. 108, pp. 2270-4, Nov 4 2003.
57. [16] R. Elghanian*, et al.*, "Selective colorimetric detection of polynucleotides based on the distance-dependent optical properties of gold nanoparticles," *Science,* vol. 277, pp. 1078-81, Aug 22 1997.
58. G. Han*, et al.*, "Functionalized gold nanoparticles for drug delivery," *Nanomedicine (Lond),* vol. 2, pp. 113-23, Feb 2007.
59. C. M. Cobley*, et al.*, "Targeting gold nanocages to cancer cells for photothermal destruction and drug delivery," *Expert Opin Drug Deliv,* vol. 7, pp. 577-87, May.
60. V. Labhasetwar, "Nanotechnology for drug and gene therapy: the importance of understanding molecular mechanisms of delivery," *Curr Opin Biotechnol,* vol. 16, pp. 674-80, Dec 2005.
61. A. Norman*, et al.*, "Cytogenetic effects of contrast media and triiodobenzoic acid derivatives in human lymphocytes," *Radiology,* vol. 129, pp. 199-203, Oct 1978.
62. F. H. Adams*, et al.*, "Effect of radiation and contrast media on chromosomes. Preliminary report," *Radiology,* vol. 124, pp. 823-6, Sep 1977.

63. P. Dawson*, et al.*, "Iodinated contrast agents as "radiosensitizers"," *Br J Radiol,* vol. 60, pp. 201-3, Feb 1987.

64. T. D. Solberg*, et al.*, "Calculation of radiation dose enhancement factors for dose enhancement therapy of brain tumours," *Phys Med Biol,* vol. 37, pp. 439-43, Feb 1992.

65. J. F. Adam*, et al.*, "Enhanced delivery of iodine for synchrotron stereotactic radiotherapy by means of intracarotid injection and blood-brain barrier disruption: quantitative iodine biodistribution studies and associated dosimetry," *Int J Radiat Oncol Biol Phys,* vol. 61, pp. 1173-82, Mar 15 2005.

66. J. F. Adam*, et al.*, "Heavy element enhanced synchrotron stereotactic radiotherapy as a promising brain tumour treatment," *Physica medica : PM : an international journal devoted to the applications of physics to medicine and biology : official journal of the Italian Association of Biomedical Physics (AIFB),* vol. 24, pp. 92-7, 2008.<Go to ISI>://MEDLINE:18407772

67. Y. Prezado*, et al.*, "Biological equivalent dose studies for dose escalation in the stereotactic synchrotron radiation therapy clinical trials," *Medical physics,* vol. 36, pp. 725-33, 2009.

68. J. Rousseau*, et al.*, "Intracerebral delivery of 5-iodo-2'-deoxyuridine in combination with synchrotron stereotactic radiation for the therapy of the F98 glioma," *Journal of synchrotron radiation,* vol. 16, pp. 573-81, 2009.<Go to ISI>://MEDLINE:19535873

69. J. E. Chang*, et al.*, "Radiotherapy and radiosensitizers in the treatment of glioblastoma multiforme," *Clin Adv Hematol Oncol,* vol. 5, pp. 894-902, 907-15, Nov 2007.

70. G. A. Viani*, et al.*, "Whole brain radiotherapy with radiosensitizer for brain metastases," *J Exp Clin Cancer Res,* vol. 28, p. 1, 2009.

71. P. Tamulevicius*, et al.*, "Misonidazole as a radiosensitizer in the radiotherapy of glioblastomas and oesophageal cancer. Pharmacokinetic and clinical studies," *Br J Radiol,* vol. 54, pp. 318-24, Apr 1981.

72. M. Sunamura*, et al.*, "Phase III trial of radiosensitizer PR-350 combined with intraoperative radiotherapy for the treatment of locally advanced pancreatic cancer," *Pancreas,* vol. 28, pp. 330-4, Apr 2004.

73. H. Sack*, et al.*, "[Postoperative radiotherapy of astrocytomas grade 3 and 4 with the radiosensitizer misonidazole. -End results of a multicentric controlled German study]," *Strahlentherapie,* vol. 158, pp. 466-9, Aug 1982.

74. A. V. Mesa*, et al.*, "Dose distributions using kilovoltage x-rays and dose enhancement from iodine contrast agents," *Phys Med Biol,* vol. 44, pp. 1955-68, Aug 1999.

75. A. Norman*, et al.*, "Contrast-enhanced brachytherapy for prostate cancer," *Acad Radiol,* vol. 9 Suppl 1, pp. S182-4, May 2002.

76. J. H. Rose*, et al.*, "First radiotherapy of human metastatic brain tumors delivered by a computerized tomography scanner (CTRx)," *Int J Radiat Oncol Biol Phys,* vol. 45, pp. 1127-32, Dec 1 1999.

77. R. Nath*, et al.*, "Dose perturbations by high atomic number materials in intravascular brachytherapy," *Cardiovasc Radiat Med,* vol. 1, pp. 144-53, Apr-Jun 1999.

78. S. H. Cho, "Estimation of tumor dose enhancement due to gold nanoparticles during typical radiation treatments: a preliminary Monte Carlo study," *Phys Med Biol,* vol. 50, pp. N163-73, Aug 7 2005.

79. D. F. Regulla*, et al.*, "Physical and biological interface dose effects in tissue due to X-ray-induced release of secondary radiation from metallic gold surfaces," *Radiat Res,* vol. 150, pp. 92-100, Jul 1998.

80. O. Ishida*, et al.*, "Size-dependent extravasation and interstitial localization of polyethyleneglycol liposomes in solid tumor-bearing mice," *Int J Pharm,* vol. 190, pp. 49-56, Nov 10 1999.

81. F. Yuan*, et al.*, "Microvascular permeability and interstitial penetration of sterically stabilized (stealth) liposomes in a human tumor xenograft," *Cancer Res,* vol. 54, pp. 3352-6, Jul 1 1994.

BIOGRAPHICAL INFORMATION

Santana Bala Lakshmanan lived in Chennai, India. In 2009, she completed her dual degree (Bachelor of Technology) in Leather and Information technology at Anna University, Chennai, India. Fall 2009, she joined the University of Texas at Arlington to pursue her masters in Materials Science and Engineering. She worked as a research assistant in Dr. Wei Chen's Nano-Bio Physics laboratory. Her area of research covered the synthesis, characterization and application of nanomaterials in cancer research.